Nonlinear saturation of the thermoacoustic instability

S. Karpov and A. Prosperetti[a)]
Department of Mechanical Engineering, The Johns Hopkins University, Baltimore, Maryland 21218

(Received 15 February 1999; accepted for publication 10 February 2000)

A weakly nonlinear theory of the thermoacoustic instability in gas-filled tubes is developed in the time domain by exploiting the difference between the instability time scale and the period of standing waves. By carrying the expansion to fourth order in the perturbation parameter, explicit results for the initial growth, nonlinear evolution, and final saturation are obtained. The dependence of the saturation amplitude upon the temperature difference in the stack, the tube geometry, stack plate spacing, Prandtl number, and other parameters is illustrated. © *2000 Acoustical Society of America.* [S0001-4966(00)03605-5]

PACS numbers: 43.35.Ud [HEB]

INTRODUCTION

The linear theory of thermoacoustic effects, as developed in the well-known series of papers by Rott (1969, 1976, 1980) is by now well established (good reviews are provided by Rott, 1983; Wheatley, 1986; and Swift, 1988). The extension of this work to the nonlinear regime is, however, a difficult task. Cao *et al.* (1996) have presented numerical solutions of the complete set of conservation equations for a simplified thermoacoustic couple at steady state. In order to refine these calculations, Worlikar *et al.* (Worlikar and Knio, 1996, 1998; Worlikar *et al.*, 1998) had to devise a new formulation leading to a manageable numerical task in spite of the scale complexity inherent to the problem.

In an earlier paper (Yuan *et al.*, 1997), we have presented numerical results based on an approximate quasi-one-dimensional extension of the linear theory. These results are interesting, but the calculations are complex and time consuming and it is difficult to carry out extensive parametric studies on their basis. For this purpose, analytic or semianalytic approximations would be more useful but, in this field, very little has been done. The only analytical work dealing with the nonlinear problem is a recent one by Gopinath *et al.* (1998), who calculated the steady temperature distribution in a resonant channel starting from a boundary layer approximation to the complete two-dimensional formulation. The problem was solved only to the extent needed to find the second-order time-independent part of the temperature field.

The purpose of the present paper is to obtain a time-domain description of the evolution of the thermoacoustic instability and to determine its saturation level and its dependence on the parameters of the problem. Thus, this work is quite different from that of Gopinath *et al.*, where the oscillations were externally forced. The complex calculations of these authors suggest that the pursuit of our objective on the basis of the exact equations might be, at least for the time being, overly ambitious. For this reason, we base our weakly nonlinear analysis on the simplified quasi-one-dimensional model developed in earlier papers (Watanabe *et al.*, 1997; Yuan *et al.*, 1997), using a method of multiple time scales similar to the one in our recent study of the linear problem (Karpov and Prosperetti, 1998). As with all such calculations, the results are valid only in a neighborhood of the instability threshold. We assume that the flow remains laminar, which is justified particularly near threshold (see, e.g., Akhavan *et al.*, 1991; Cooper *et al.*, 1993).

In a typical prime mover arrangement, it is only the fundamental mode that is unstable, while the higher-order modes are stable. In order for the instability to saturate, therefore, it is necessary that the energy injected into the fundamental mode be transferred by nonlinear couplings to the higher modes, where it is dissipated. Since the energy input is proportional to the square of the amplitude of the fundamental, while the energy dissipation is proportional to the square of the amplitude of the higher modes which, due to the nonlinearity, are at least quadratic in the amplitude of the fundamental, at sufficiently high amplitudes a balance is reached that allows the system to reach steady state.

The mathematical model that we use contains a great deal of information on the geometry and other characteristics of the system. Our results are therefore useful to explore the dependence of both the transient and the steady state on these parameters. As a demonstration, we show the dependence of the saturation amplitude on the temperature difference in the stack, the separation of the stack plates, the gas Prandtl number, and other quantities. In particular, it is found that the system is extremely sensitive to the shape of the resonant tube, which determines the mutual relation among the modes and therefore the ease with which energy can be transferred from the fundamental to the higher modes.

I. MATHEMATICAL MODEL

In Watanabe *et al.* (1997), a nonlinear model for thermoacoustic devices was derived by averaging the exact conservation equations for mass, momentum, and energy over the cross section of the device. The model consists of the equations of continuity

$$\frac{\partial \rho}{\partial \hat{t}} + \frac{1}{S}\frac{\partial}{\partial x}(S\rho u) = 0, \tag{1.1}$$

momentum

a)Electronic mail: prosperetti@jhu.edu

$$\rho \frac{\partial u}{\partial \hat{t}} + \rho u \frac{\partial u}{\partial x} + \frac{\partial p}{\partial x} = -\mathcal{D}(u), \tag{1.2}$$

and energy

$$\frac{\partial p}{\partial \hat{t}} + u \frac{\partial p}{\partial x} + \frac{\gamma p}{S} \frac{\partial (Su)}{\partial x} = (\gamma - 1)\left[\mathcal{H}(T_w - T) - \frac{dT_w}{dx} \mathcal{Q}(u) + u\mathcal{D}(u) \right] \tag{1.3}$$

supplemented by the perfect-gas equation of state

$$p = \mathcal{R}\rho T. \tag{1.4}$$

In these equations $\hat{t}$ is the dimensional time, ρ, p, T, and u are the cross-sectional averages of the density, pressure, temperature, and velocity fields of the gas, respectively and T_w is the prescribed temperature of the solid surfaces in contact with the gas, i.e., the tube walls and the stack plates. Unlike Gopinath *et al.* (1998), who were interested in the temperature distribution caused by a prescribed acoustic field, our focus here is on the evolution of the acoustic field under the destabilizing action of an externally imposed wall temperature gradient. For this reason, and in view of the large thermal capacity of typical stack plates, for simplicity we assume that $T_w = T_w(x)$ is a prescribed function of x. With relatively straightforward adjustments, however, the present method can be extended to deal with a T_w dependent on time over the fast time scale of the acoustic oscillations as well as over the slower time scale of the developing instability. The spatial coordinate x is directed along the axis of the device, $S(x)$ is the (in general, nonuniform) cross-sectional area, γ the ratio of specific heats, and $\mathcal{R}$ the universal gas constant divided by the gas molecular mass.

The key to the success of the model (1.1) to (1.4) lies in the proper specification of the operators $\mathcal{D}$, $\mathcal{H}$, and $\mathcal{Q}$ that account for the exchange of momentum and energy between the gas and the solid surfaces in contact with it. In the model of Watanabe *et al.* (1997), these quantities were specified in such a way that the resulting theory, upon linearization, became identical to the exact linear theory developed by Rott (1969, 1983; see also Swift, 1989). Here, we deviate in two significant aspects from our earlier work. In the first place, since the nature of the perturbation method that we use enables us to distinguish between different Fourier components of the solution, we do not need to commit ourselves to a frequency-independent form for the operators. Second, while in the previous paper we extended the original definition of the operators to the nonlinear domain, here we retain their linear form. The motivation is not only one of simplicity but also, as mentioned at the end of Sec. IV, the fact that both numerical and perturbation results obtained with and without the nonlinear extension are very close. This circumstance is fortunate in view of the uncertainty affecting their proper extension to the nonlinear regime.

Using the forms of $\mathcal{H}$ and $\mathcal{Q}$ given in our previous paper (Watanabe *et al.*, 1997), in the linear approximation, we have

$$\mathcal{T}(p', u') \equiv \mathcal{H}(T_w - T) - \frac{dT_w}{dx} \mathcal{Q}(u') = -i\hat{\omega} f_K p' - \rho_0 c_p \frac{f_V - f_K}{(1 - f_V)(1 - \sigma)} \frac{dT_w}{dx} u', \tag{1.5}$$

where primes denote linear perturbation values, i.e., $p' = p - p_0$, with p_0 the undisturbed pressure. This expression has been written in the frequency domain and a dependence of p' and u' proportional to $\exp i\hat{\omega}t$ is implied. The parameters $f_{V,K}$ depend on the ratio of the diffusion lengths $\delta_{V,K}$ to the plate spacing l and are given by (Swift, 1988)

$$f = (1 - i)\frac{\delta}{l} \tanh(1 + i)\frac{l}{2\delta}, \tag{1.6}$$

where the index can be V or K. The viscous and thermal penetration lengths $\delta_{V,K}$ are given by

$$\delta_V = \sqrt{\frac{2\nu}{\hat{\omega}}}, \quad \delta_K = \sqrt{\frac{2\alpha}{\hat{\omega}}} = \frac{\delta_V}{\sqrt{\sigma}}, \tag{1.7}$$

with ν the kinematic viscosity, σ the Prandtl number, and $\alpha = \nu/\sigma$ the thermal diffusivity. For a circular cross section with radius r_0, one has instead (Rott, 1969)

$$f = \frac{2J_1((i-1)(r_0/\delta))}{(i-1)(r_0/\delta)J_0((i-1)(r_0/\delta))}, \tag{1.8}$$

again valid for both f_V and f_K. When the diffusion penetration depths are small compared with either l or r_0, f given by either (1.6) or (1.8) admits the asymptotic approximation

$$f \simeq (1 - i)\frac{\delta}{l}, \quad f \simeq (1 - i)\frac{\delta}{r_0}. \tag{1.9}$$

More generally, for other cross-section shapes, in this limit one may set $f \simeq 2(1 - i)\delta/d_h$, where $d_h = 4S(x)/s(x)$ is the hydraulic diameter defined in terms of the cross-sectional area S and the ''wetted'' perimeter s. The action of the wall drag operator $\mathcal{D}$ is expressed similarly

$$\mathcal{D}(u') = i\rho_0\hat{\omega}\frac{f_V}{1 - f_V}u'. \tag{1.10}$$

We reiterate that, upon linearization, in the frequency domain the previous model reduces exactly to Rott's formulation.

II. ASYMPTOTIC ANALYSIS

In setting up a perturbation approach to the problem posed in the previous section, we note that experiment (see, e.g., Wheatley, 1986; Atchley, 1990) shows that the initial build-up of the thermoacoustic instability has the character of a modulated standing wave, the frequency of which is essentially dictated by the resonator, while the amplitude is slowly varying in time. Similarly, if the thermoacoustic device is driven externally by a loudspeaker or a piston, the steady-state temperature distribution evolves slowly over the time scale of the acoustic period. These observations suggest the possibility of setting up a perturbation scheme based on

the smallness of the ratio of the characteristic period of oscillation to the characteristic time for the evolution of the thermoacoustic effect.

In the framework of the previous model, the terms in the left-hand side of Eqs. (1.1)–(1.3) describe nonlinear oscillations in a gas column with variable cross-sectional area and temperature stratification and are therefore responsible for the ''carrier'' frequency of the wave. The heart of the thermoacoustic effect is in the terms in the right-hand sides. The observed slowness of the modulation implies that the effect of these terms is small. As will be seen in the following, this effect arises through integrals over the tube length. Therefore, the effect will be small not only when the terms themselves are small but—as usually happens in practice—when they are large only over a small fraction of the tube length. A formal justification of this statement will be found in Appendix A. In order to set up a perturbation scheme, we introduce a small parameter ϵ and set

$$F_K=\frac{f_K}{\epsilon}, \quad F_Q=\frac{1}{\epsilon}\frac{f_V-f_K}{(1-f_V)(1-\sigma)}, \quad F_D=\frac{1}{\epsilon}\frac{f_V}{1-f_V}, \tag{2.1}$$

with $F_{K,Q}$ formally treated as $O(1)$ quantities. The considerations of Appendix A show that this does not necessarily imply that the f's are of order ϵ, but only that

$$\frac{L_S}{L} f_{V,K} \sim \epsilon, \tag{2.2}$$

where L_S is the length of the stack region, i.e., the region where the f's are not small. An explicit definition of ϵ is not necessary as the final results do not explicitly depend on this parameter, but one may think of it as the ratio of the standing wave period to the modulation time scale.

We use the method of multiple time scales (see, e.g., Kevorkian and Cole, 1996; Murdock, 1991; Hinch, 1991) and introduce the new time variables

$$t=\hat{t}, \quad \tau=\epsilon\hat{t}, \quad \theta=\epsilon^2\hat{t}, \quad \eta=\epsilon^3\hat{t}. \tag{2.3}$$

As a consequence of these definitions, we have

$$\frac{\partial}{\partial\hat{t}}=\frac{\partial}{\partial t}+\epsilon\frac{\partial}{\partial\tau}+\epsilon^2\frac{\partial}{\partial\theta}+\epsilon^3\frac{\partial}{\partial\eta}+\cdots. \tag{2.4}$$

The field variables are also expanded in a power series in ϵ; for example

$$p'(x,\hat{t})=\epsilon p_1(x,\hat{t})+\epsilon^2 p_2(x,\hat{t})+\epsilon^3 p_3(x,\hat{t})+\epsilon^4 p_4(x,\hat{t})+\cdots, \tag{2.5}$$

with analogous expressions for u', etc. These expansions imply that the nonlinearity is taken to be of the same order as the amplitude modulation, which is the interesting case. Indeed, if the modulation were much stronger than the nonlinearity, we would essentially be dealing with the linear problem already studied in our earlier paper (Karpov and Prosperetti, 1998). On the other hand, since the wave exists only due to the thermoacoustic instability, one cannot have a strong nonlinearity coupled with weak thermoacoustic effects.

For clarity, it is important to stress two important aspects in which the work described in this paper differs from most other nonlinear stability studies. In the first place, while the deviation from marginal stability conditions is usually measured by a single control variable, here it is a whole function—the wall temperature distribution T_w—that determines the stability properties of the linear system. The situation might be reduced to the more usual one by assuming that the temperature distribution in the stack has a certain functional form dependent upon one parameter which would then play the role of control variable. For example, a linear temperature distribution would be characterized by the temperature gradient. Such an assumption is, however, unnecessarily restrictive and it is preferable to keep the framework general.

Second, perturbation expansions are usually carried out in the neighborhood of linear marginal stability conditions that are known exactly. In order to proceed in this way, we would have to solve the linear problem including the exchange terms $f_{V,K}$, find the marginal stability conditions, and then allow for a perturbation. Here, such a procedure would not lead to very transparent results given the complexity of the linear problem, compounded by the fact that, with nonzero f's, the linear operator is not self-adjoint. Hence, we prefer to take a different approach choosing as our base state the situation in which there is no coupling between the gas and the solid structure even though, in general, this situation is not marginally stable. The marginal stability condition will be determined as part of the perturbation procedure itself, much as in our earlier paper (Karpov and Prosperetti, 1998), of which the first few steps of the present perturbation procedure constitute a refinement.

Here, therefore, as the parameter ϵ is increased from zero, two effects appear: the coupling with the solid structure dampens or amplifies the oscillations, and nonlinear effects influence their development. It will be seen that the first effect sets in at a lower order in ϵ than the second one. The first few steps of the perturbation procedure, therefore, furnish successively closer approximations to the linear stability threshold, from which the nonlinear effects eventually take off.

In order to deal with this situation we must clarify the role played by the wall temperature distribution $T_w(x)$. In the usual perturbation procedures, the small parameter is the difference between the given value of the control variable and the critical value. Here, we deal with the function T_w, and the critical conditions are not known exactly. Thus, we represent the given function T_w as

$$T_w(x)=T_{w0}(x)+\epsilon T_{w1}(x)+\epsilon^2 T_{w2}(x). \tag{2.6}$$

The terms T_{w0}, T_{w1} will be determined so as to satisfy the marginal stability conditions, after which the difference $T_w(x)-[T_{w0}(x)+\epsilon T_{w1}(x)]$ will be the driving force for the development of the instability to the order considered.[1] In principle, the same procedure can be applied to higher orders in ϵ. Since the appearance of the instability depends on integral conditions on the T_{wj}'s, in principle, there is a degree of nonuniqueness here since the T_{wj}'s can be taken arbitrarily, provided only the integral conditions are satisfied. In spite of

this seeming level of arbitrariness, one would expect the results to be insensitive to any specific choice, and indeed we have verified this numerically as will be described below.

From (2.6), we also have

$$\frac{dT_w}{dx} = G_0 + \epsilon G_1 + \epsilon^2 G_2, \tag{2.7}$$

where

$$G_j = \frac{dT_{wj}}{dx}, \quad j = 0,1,2,\ldots. \tag{2.8}$$

Furthermore, since the equilibrium density is connected to p_0 and T_w by the equation of state, when we write

$$\rho(x,\hat{t}) = \rho_0 + \epsilon\rho_1(x,\hat{t}) + \epsilon^2\rho_2(x,\hat{t}) + \epsilon^3\rho_3(x,\hat{t}) + \epsilon^4\rho_4(x,\hat{t}) + \cdots, \tag{2.9}$$

the corrections ρ_1, etc. will contain time-independent components related to T_{w1}, etc. With all these definitions we may write

$$\mathcal{T}(p',u') = \epsilon^2\mathcal{T}_1 + \epsilon^3\mathcal{T}_2 + \epsilon^4\mathcal{T}_3, \tag{2.10}$$

$$\mathcal{D}(u') = \epsilon^2\mathcal{D}_1 + \epsilon^3\mathcal{D}_2 + \epsilon^4\mathcal{D}_3, \tag{2.11}$$

where

$$\mathcal{T}_1 = -i\omega F_K p_1 - \rho_0 c_p F_Q G_0 u_1, \quad \mathcal{D}_1 = i\rho_0\omega F_V u_1, \tag{2.12}$$

etc.

All the expansions, together with (2.4), are substituted into Eqs. (1.1)–(1.4) and the various orders in ϵ are separated, giving rise to a sequence of problems that we describe separately. Many of the details of the calculation can be found in Appendix B. Only a streamlined summary of the procedure is described here.

A. Order zero

At order zero the solution is

$$u_0 = 0, \tag{2.13}$$

with p_0 and $T_0 = T_{w0}(x)$ arbitrary but regarded as given.

B. First order

The problem to order one was studied in an earlier paper (Karpov and Prosperetti, 1998) and the details will be omitted here. The equations are

$$\frac{\partial\rho_1}{\partial t} + \frac{1}{S}\frac{\partial}{\partial x}(S\rho_0 u_1) = 0, \tag{2.14}$$

$$\rho_0\frac{\partial u_1}{\partial t} + \frac{\partial p_1}{\partial x} = 0, \tag{2.15}$$

$$\frac{\partial p_1}{\partial t} + \frac{\gamma p_0}{S}\frac{\partial(Su_1)}{\partial x} = 0, \tag{2.16}$$

and the pressure field is found to be

$$p_1 = A(\tau,\theta,\eta)P_1(x)\exp(i\omega t) + \text{c.c.}, \tag{2.17}$$

where A is the slowly varying amplitude, c.c. denotes the complex conjugate, and P_1 is the solution of

$$\frac{1}{S}\frac{d}{dx}\left(c_0^2(x)S\frac{dP_1}{dx}\right) + \omega^2 P_1 = 0, \tag{2.18}$$

where

$$c_0^2(x) = \gamma\mathcal{R}T_{w0}(x), \tag{2.19}$$

is the local adiabatic sound speed.

The way in which T_{w0} is to be understood needs some clarifications, which amplify the comments made before Eq. (2.6). Let us consider first the case in which a certain temperature distribution $T_w(x)$ is prescribed. If one plans to study only the linear problem, T_{w0} can be taken as the given T_w. On the other hand, if the plan is to carry the expansion to include nonlinear effects, as will be discussed below, T_{w0} must be determined (or, at least, constrained) using the results of the next step in the perturbation procedure. Finally, if the objective is the determination of the onset temperature distribution, $T_w(x)$ is unknown at the outset, and the T_{w0} appearing in (2.18) is its first approximation that will be determined at the next step. Actually, the last two possibilities are one and the same as, if one plans to carry the expansion to include nonlinear effects, one needs to determine the onset temperature distribution first. A consequence of the indeterminacy of T_{w0} at this stage is an indeterminacy of ρ_0, which will be determined from the equation of state $\mathcal{R}\rho_0 T_{w0} = p_0$ once T_{w0} is found.

We take the tube to be rigidly terminated at the ends, and therefore impose that

$$\frac{dP_1}{dx} = 0 \quad \text{at} \quad x = 0, \quad x = L, \tag{2.20}$$

which ensure that the eigenvalue ω^2 is real and positive (see, e.g., Morse and Feshbach, 1953, p. 728; Naylor and Sell, 1982, p. 502). The eigenfunction P_1 can therefore also be taken real and, for later convenience, we normalize it so that

$$\int_0^L S(x)P_1^2(x)dx = Vp_0^2, \tag{2.21}$$

where V is the volume of the device.

In deriving an expression for the gas density to this order, we anticipate the fact that, at the next order, we will encounter a contribution T_{w1} that will affect the undisturbed value of ρ. Hence, we write

$$\rho_1 = \rho_{10} + \rho_{11}, \tag{2.22}$$

where ρ_{10} will be determined at the third step from the equation of state

$$\mathcal{R}(\rho_0 + \epsilon\rho_{10})(T_{w0} + \epsilon T_{w1}) = p_0. \tag{2.23}$$

The term ρ_{11} is instead associated to p_1 and can be found from (2.14) to (2.16), together with u_1. The dependence of both quantities on the time variables and the perturbation amplitude A is the same as (2.17), and the spatial dependence is given by

$$R_1(x) = -\frac{1}{\omega^2 S}\frac{d}{dx}\left(S\frac{dP_1}{dx}\right), \tag{2.24}$$

$$U_1(x)=\frac{i}{\omega\rho_0}\frac{dP_1}{dx}. \tag{2.25}$$

C. Second order

As shown in Appendix B, at second order one finds the following equation for p_2:

$$\frac{\partial^2 p_2}{\partial t^2}-\frac{1}{S}\frac{\partial}{\partial x}\left(c_0^2 S\frac{\partial p_2}{\partial x}\right)=(\mathrm{RHS})_2, \tag{2.26}$$

where c_0^2 is defined in (2.19) and

$$\begin{aligned}(\mathrm{RHS})_2=&(\gamma-1)\frac{\partial \mathcal{T}_1}{\partial t}-2\frac{\partial^2\rho_1}{\partial t\partial\tau}\\&-\frac{\partial}{\partial t}\left[u_1\frac{\partial p_1}{\partial x}+\frac{\gamma p_1}{S}\frac{\partial}{\partial x}(Su_1)\right]\\&+\frac{\gamma p_0}{S}\frac{\partial}{\partial x}S\left[\frac{1}{\rho_0}\mathcal{D}_1+u_1\frac{\partial u_1}{\partial x}+\frac{\rho_1}{\rho_0}\frac{\partial u_1}{\partial t}\right].\end{aligned} \tag{2.27}$$

The forcing at frequencies $\pm\omega$ in the right-hand side will generate resonant terms proportional to $t\exp(\pm i\omega t)$ in the solution for p_2 which would lead to a breakdown of the approximation over times of order $(\epsilon\omega)^{-1}$. To avoid this resonance, as in the standard procedure (Kevorkian and Cole, 1996; Murdock, 1991; Hinch, 1991), we impose the solvability condition that the right-hand side of the equation be orthogonal to the solutions of the (adjoint) homogeneous equation, namely $\exp(\pm i\omega t)P_1$

$$\int_0^{2\pi/\omega}dt\int_0^L S[\exp(\mp i\omega t)P_1](\mathrm{RHS})_2 dx=0. \tag{2.28}$$

Multiplication by $S(x)$ before integration is necessary so that the x operator in the left-hand side of (2.26) be self-adjoint with the boundary conditions (2.20). The two conditions (2.28) give

$$\frac{\partial A}{\partial\tau}-i\Omega_1 A=0, \tag{2.29}$$

plus its complex conjugate, where

$$\begin{aligned}\Omega_1=&-\frac{1}{2Vp_0^2\omega}\int_0^L S\left[c_0^2\left(F_D+\frac{\rho_{10}}{\rho_0}\right)\left(\frac{dP_1}{dx}\right)^2\right.\\&\left.+(\gamma-1)\omega^2F_K P_1^2+(\gamma-1)c_pF_Q G_0P_1\frac{dP_1}{dx}\right]dx.\end{aligned} \tag{2.30}$$

The solution of (2.29) is

$$A(\tau,\theta,\eta)=B(\theta,\eta)\exp(i\Omega_1\tau), \tag{2.31}$$

which increases exponentially if $\mathrm{Im}\,\Omega_1<0$. It will be noted that $\mathrm{Im}\,\Omega_1$ exists only due to the F terms that account for momentum and energy exchange with the solid structure and is therefore not affected by the indeterminacy of ρ_{10} at this stage of the calculation. It will be seen below that, in order to continue the perturbation scheme into the nonlinear domain, for consistency it is necessary to have $\mathrm{Im}\,\Omega_1=0$, which is a constraint on G_0 and, therefore, T_{w0}. This constraint can of course be met in an infinity of ways, although one would not expect any particular choice to have consequences for the remainder of the calculation provided the choice is such that $T_w-T_{w0}=O(\epsilon)$, in keeping with (2.6). Indeed, as will be shown below, this is in agreement with our numerical evidence.

In our earlier paper (Karpov and Prosperetti, 1998) we gave explicit expressions for the onset temperature gradient G_0 on the assumption that it is constant in the stack. By means of the short-stack approximation, it was possible to derive simple formulas that generalize the concept of critical gradient of elementary theory to the presence of viscous effects and narrow gaps.

When (2.28) is satisfied, one can look for the solution of Eq. (2.26) for p_2 in the form of the superposition of terms at frequencies 0, $\pm\omega$, and $\pm 2\omega$, respectively

$$p_2=AP_{21}(x)e^{i\omega t}+A^2P_{22}(x)e^{2i\omega t}+A^*AP_{20}(x)+\mathrm{c.c.} \tag{2.32}$$

Here, the asterisk denotes the complex conjugate. The equations for $P_{21}(x)$, $P_{22}(x)$, and $P_{20}(x)$ are obtained from Eq. (2.26) upon separating the different frequency components in the right-hand side. However, P_{20} is more easily determined from the momentum equation (B5). The explicit form of these equations is given in (B7)–(B9) in Appendix B.

D. Third order

Proceeding as before, at the third order we find

$$\frac{\partial^2 p_3}{\partial t^2}-\frac{1}{S}\frac{\partial}{\partial x}\left(c_0^2 S\frac{\partial p_3}{\partial x}\right)=(\mathrm{RHS})_3, \tag{2.33}$$

where

$$\begin{aligned}(\mathrm{RHs})_3=&(\gamma-1)\frac{\partial}{\partial t}(\mathcal{T}_2+u_1\mathcal{D}_1)-2\frac{\partial^2 p_1}{\partial t\partial\theta}-\frac{\partial^2 p_2}{\partial t\partial\tau}\\&-\frac{\partial}{\partial t}\left(u_1\frac{\partial p_2}{\partial x}+u_2\frac{\partial p_1}{\partial x}+\frac{\gamma p_1}{S}\frac{\partial(Su_2)}{\partial x}\right.\\&\left.+\frac{\gamma p_2}{S}\frac{\partial(Su_1)}{\partial x}\right)+\frac{1}{S}\frac{\partial(Sc_0^2\mathcal{D}_2)}{\partial x}+\frac{\gamma p_0}{S}\frac{\partial}{\partial x}\\&\times\left(S\left[\frac{\partial u_2}{\partial\tau}+\frac{\partial(u_1u_2)}{\partial x}+\frac{\rho_1}{\rho_0}\left(\frac{\partial u_2}{\partial t}+\frac{\partial u_1}{\partial\tau}+u_1\frac{\partial u_1}{\partial x}\right)\right.\right.\\&\left.\left.+\frac{\rho_2}{\rho_0}\frac{\partial u_1}{\partial t}\right]\right).\end{aligned} \tag{2.34}$$

The solvability condition is again (2.28), which leads to

$$\frac{\partial A}{\partial\theta}-i(\Omega_2+\Lambda_2|A|^2)A=0, \tag{2.35}$$

where

$$\Omega_2=\frac{1}{2\omega_0 Vp_0^2}\int_0^L Sc_0^2\frac{dP_1}{dx}\left[\left(F_D^2+F_D\frac{\rho_{10}}{\rho_0}+\frac{T_{w2}}{T_{w0}}\right)\frac{dP_1}{dx}-\left(F_D+\frac{\rho_{10}}{\rho_0}\right)\frac{dP_{21}}{dx}\right]dx-\frac{\Omega_1^2}{2\omega}-\frac{\gamma-1}{2\omega Vp_0^2}\int_0^L SP_1\left[2\omega\Omega_1F_KP_1+\omega^2F_KP_{21}+c_pF_QG_1\frac{dP_1}{dx}+c_pF_QG_0\left(\frac{dP_{21}}{dx}-F_D\frac{dP_1}{dx}\right)\right]dx, \tag{2.36}$$

$$\Lambda_2=\frac{i}{2Vp_0^2}\int_0^L SP_1\left[U_1\left(2\frac{dP_{20}}{dx}-\frac{dP_{22}}{dx}\right)+U_{22}\frac{dP_1}{dx}+\frac{\gamma P_1}{S}\frac{d(SU_{22})}{dx}+\frac{\gamma}{S}(2P_{20}-P_{22})\frac{d(SU_1)}{dx}\right]dx-\frac{\gamma p_0}{2\omega_0 Vp_0^2}\int_0^L S\frac{dP_1}{dx}\left[U_1\frac{dU_{22}}{dx}+U_{22}\frac{dU_1}{dx}+\frac{R_1}{\rho_0}\times\left(U_1\frac{dU_1}{dx}-2i\omega U_{22}\right)-\left(\frac{R_{22}}{\rho_0}+2\frac{P_{20}}{p_0}\right)i\omega U_1\right]dx. \tag{2.37}$$

Since in Λ_2 all the U's are pure imaginary while the P's are real, this quantity is real. On the other hand, Ω_2 is complex in general but becomes real in neutrally stable conditions where $\mathrm{Im}\,\Omega_2=0$ gives the second approximation to the onset critical gradient.

Upon substituting into (2.35) Eq. (2.31) for A, we have

$$\frac{\partial B}{\partial\theta}-i[\Omega_2+\Lambda_2|B|^2\exp(-2\,\mathrm{Im}\,\Omega_1\tau)]B=0. \tag{2.38}$$

Since, by hypothesis, B cannot depend on τ, this equation is only consistent provided $\mathrm{Im}\,\Omega_1=0$, which, as noted before, ensures that the temperature gradient corresponds to the onset value at this level of approximation. This consistency condition motivated the expansion of T_w into the series of terms (2.6) to be chosen so that the condition can be satisfied. When $\mathrm{Im}\,\Omega_1=0$, then we have

$$B(\theta,\eta)=C(\eta)\exp(i[\Omega_2+\Lambda_2|C|^2]\theta), \tag{2.39}$$

The solution p_3 is given by

$$p_3=(AP_{311}(x)+A^*A^2P_{313})e^{i\omega t}+A^2P_{32}(x)e^{2i\omega t}+A^3P_{33}(x)e^{3i\omega t}+A^*AP_{30}(x)+\text{c.c.} \tag{2.40}$$

The equations for $P_{311}(x)$, $P_{313}(x)$, $P_{32}(x)$, and $P_{30}(x)$ are given in (B28)–(B32) of Appendix B.

E. Fourth order

At fourth order we find

$$\frac{\partial^2 p_4}{\partial t^2}-\frac{1}{S}\frac{\partial}{\partial x}\left(c_0^2S\frac{\partial p_4}{\partial x}\right)=(\mathrm{RHS})_4, \tag{2.41}$$

where

$$(\mathrm{RHS})_4=-2\frac{\partial^2 p_1}{\partial t\partial\eta}-\frac{\partial^2 p_2}{\partial t\partial\theta}-\frac{\partial^2 p_3}{\partial t\partial\tau}+(\gamma-1)\frac{\partial}{\partial t}(\mathcal{T}_3+u_1\mathcal{D}_2+u_2\mathcal{D}_1)-\frac{\partial}{\partial t}\left(u_1\frac{\partial p_3}{\partial x}+u_2\frac{\partial p_2}{\partial x}+u_3\frac{\partial p_1}{\partial x}+\frac{\gamma}{S}\left(p_1\frac{\partial(Su_3)}{\partial x}+p_2\frac{\partial(Su_2)}{\partial x}+p_3\frac{\partial(Su_1)}{\partial x}\right)\right)+\frac{\gamma p_0}{S}\frac{\partial}{\partial t}\left(S\left[\frac{1}{\rho_0}\mathcal{D}_3+\frac{\partial u_3}{\partial\tau}+\frac{\partial u_2}{\partial\theta}+\frac{\rho_1}{\rho_0}\left(\frac{\partial u_3}{\partial t}+\frac{\partial u_2}{\partial\tau}+\frac{\partial u_1}{\partial\theta}+\frac{\partial(u_1u_2)}{\partial x}\right)+\frac{\rho_2}{\rho_0}\left(\frac{\partial u_2}{\partial t}+\frac{\partial u_1}{\partial\tau}+u_1\frac{\partial u_1}{\partial x}\right)+\frac{\rho_3}{\rho_0}\frac{\partial u_1}{\partial t}+\frac{\partial(u_1u_3)}{\partial x}+u_2\frac{\partial u_2}{\partial x}\right]\right). \tag{2.42}$$

For the purpose of extracting the slow time evolution of the disturbance amplitude, we only need the part of $(\mathrm{RHS})_4$ proportional to $\exp\pm i\omega t$, on which the solvability condition (2.28) is to be imposed. The result is

$$\frac{dC}{d\eta}-i[\Omega_3+\Lambda_3|C|^2\exp(-2\,\mathrm{Im}\,\Omega_2\theta)]C=0, \tag{2.43}$$

together with its complex conjugate. Here,

$$\Omega_3=\frac{i}{2\omega Vp_0^2}\int_0^L Sc_0^2\frac{dP_1}{dx}[F_DU_{311}+(\Omega_1\rho_0+\rho_{10})(U_{311}+F_DU_{21})+(\Omega_2\rho_0+\Omega_1\rho_{10}+\omega\rho_{200})(U_{21}+F_DU_1)+(\Omega_2\rho_{10}+\Omega_1\rho_{200}+\omega\rho_{300})U_1]dx+\frac{i(\gamma-1)}{2Vp_0^2}\int_0^L SP_1[iF_K(\omega P_{311}+\Omega_1P_{21}+\Omega_2P_1)+c_pF_Q(\rho_0G_0U_{311}+(\rho_0G_1+\rho_{10}G_0)U_{21}+(\rho_0G_2+\rho_{10}G_1+\rho_{200}G_0)U_1)]dx, \tag{2.44}$$

$$\Lambda_3=\frac{i}{2Vp_0^2}\int_0^L SP_1\Bigg[2U_1\frac{d}{dx}(\mathrm{Re}\,P_{30})-U_1\frac{dP_{32}}{dx}+U_{21}^*\frac{dP_{22}}{dx}+2U_{21}\frac{dP_{20}}{dx}+U_{22}\frac{dP_{21}^*}{dx}+U_{32}\frac{dP_1^*}{dx}+2U_{30}\frac{dP_1}{dx}\Bigg]dx$$
$$+\frac{i\gamma}{2Vp_0^2}\int_0^L P_1\Bigg[(2\,\mathrm{Re}\,P_{30}-P_{32})\frac{d(SU_1)}{dx}+2P_{20}\frac{d(SU_{21})}{dx}+P_{22}\frac{d(SU_{21}^*)}{dx}+P_{21}^*\frac{d(SU_{22})}{dx}+2P_1\frac{d(SU_{30})}{dx}$$
$$+P_1\frac{d(SU_{32})}{dx}\Bigg]dx+\frac{i\gamma}{2Vp_0^2}\int_0^L SP_1\Bigg[iF_K(\omega P_{313}+\Lambda_2P_1)+c_pF_QG_0(\rho_0U_{313}+\rho_{202}U_1)+(F_D^*-2F_{2D})\frac{dP_1}{dx}U_{22}\Bigg]dx$$
$$+\frac{i\gamma p_0}{2Vp_0^2}\int_0^L S\frac{dP_1}{dx}\Bigg[\left(\frac{\Omega_1}{\omega}+\frac{\rho_{10}}{\rho_0}+F_D\right)U_{313}+2\frac{R_1}{\rho_0}U_{32}+\left(\frac{\Lambda_2}{\omega}+\frac{\rho_{202}}{\rho_0}\right)U_{21}-\frac{R_{22}}{\rho_0}U_{21}^*+2\left(\frac{R_{21}^*}{\rho_0}+\frac{R_1}{\rho_0}\frac{\Omega_1}{\omega}\right)U_{22}$$
$$+\left(\frac{\rho_{302}}{\rho_0}+\frac{R_{32}}{\rho_0}+\left(\frac{\rho_{10}}{\rho_0}+F_D\right)\frac{\Lambda_2}{\omega}+\left(\frac{\rho_{202}}{\rho_0}+\frac{R_{22}}{\rho_0}\right)\frac{\Omega_1}{\omega}+\frac{\rho_{202}}{\rho_0}F_D\right)U_1\Bigg]dx$$
$$+\frac{\gamma p_0}{2\omega Vp_0^2}\int_0^L S\frac{dP_1}{dx}\Bigg[\frac{d(U_{21}^*U_{22})}{dx}-\frac{d(U_1U_{32})}{dx}+\frac{R_1}{\rho_0}\left(U_1\frac{dU_{21}^*}{dx}-U_{21}\frac{dU_1}{dx}\right)-\frac{\rho_{10}}{\rho_0}\frac{d(U_1U_{22})}{dx}$$
$$+2U_1\frac{dU_{30}}{dx}-\frac{R_{21}}{\rho_0}U_1\frac{dU_1}{dx}\Bigg]dx. \tag{2.45}$$

As before in (2.38), Eq. (2.43) is only consistent if $\mathrm{Im}\,\Omega_2=0$.

III. RESULTS

The key result of the calculation described in the previous section is a relation governing the growth of the amplitude of the perturbation. Upon introducing the unscaled amplitude $\tilde{A}=\epsilon A\exp(i\omega t)$, from (2.29), (2.38), (2.43), we have

$$\frac{d\tilde{A}}{d\hat{t}}=i[(\omega+\tilde{\Omega}_1+\tilde{\Omega}_2+\tilde{\Omega}_3)+(\tilde{\Lambda}_2+\tilde{\Lambda}_3)|\tilde{A}|^2]\tilde{A}, \tag{3.1}$$

where $\tilde{\Omega}_1$ is obtained by multiplying (2.30) by ϵ,

$$\tilde{\Omega}_1=-\frac{1}{2Vp_0^2\omega}\int_0^L dx\,S\Bigg[c_0^2\left(\frac{f_V}{1-f_V}+\frac{\rho_{10}}{\rho_0}\right)\left(\frac{dP_1}{dx}\right)^2$$
$$+(\gamma-1)\omega^2f_KP_1^2+\frac{(\gamma-1)(f_V-f_K)}{(1-\sigma)(1-f_V)}c_pG_0P_1\frac{dP_1}{dx}\Bigg], \tag{3.2}$$

with similar expressions for $\tilde{\Omega}_k=\epsilon^k\Omega_k$ obtained from (2.36) and (2.44) and $\tilde{\Lambda}_k=\epsilon^k\Lambda_k$ from (2.37), (2.45).

Equation (3.1) contains both linear and nonlinear contributions that are better discussed separately. In all the numerical examples that follow, we use as reference case the geometry of the experiment of Atchley *et al.* (1990), the implementation of which in the context of the present mathematical model is described in detail in an earlier paper (Yuan *et al.*, 1997). Briefly, the system consists of a 38.2-mm-diameter tube with a length of 99.89 cm, a 35-mm-long stack of stainless-steel plates located 87.95 cm from the cold end, and two heat exchangers. The operating pressure was $p_0=307$ kPa.

A. Linear regime

In the linear approximation, Eq. (3.1) is

$$\frac{d\tilde{A}}{dt}=i(\omega+\tilde{\Omega}_1+\tilde{\Omega}_2+\tilde{\Omega}_3)\tilde{A}. \tag{3.3}$$

A consideration of Eqs. (2.38) and (2.43) shows that, for the linear problem, one can allow nonzero imaginary parts for Ω_1 and Ω_2. For this reason, it is not necessary to expand T_w in a perturbation series. Accordingly, in the previous expressions, one can set $T_{w0}=T_w$, $T_{w1}=T_{w2}=0$, $G_0=dT_w/dx$, $G_1=G_2=0$; furthermore, all time-independent corrections to ρ due to the T_{wj}'s, i.e., ρ_{10}, ρ_{200}, ρ_{300}, vanish. In addition to giving the growth rate of the perturbation for a given temperature distribution T_w, Eq. (3.3) can be used to determine onset conditions by adjusting the temperature distribution in such a way that $\mathrm{Im}(\tilde{\Omega}_1+\tilde{\Omega}_2+\tilde{\Omega}_3)=0$.

The results found in this way may be considered as a higher-order extension of those presented in our previous paper (Karpov and Prosperetti, 1998) where only the expression for $\tilde{\Omega}_1$ was given. In that study, we showed that this result of relatively low order of accuracy is already in excellent agreement with Rott's exact linear theory prediction. Equation (3.3) can therefore be considered a higher-order approximation to Rott's theory and indeed we have confirmed this expectation by evaluating numerically $\tilde{\Omega}_2$ and $\tilde{\Omega}_3$. A typical example is shown in Fig. 1, where the imaginary part of the exact linear eigenfrequency—i.e., minus the growth rate of the instability—(solid line) is compared with the successive approximations $\mathrm{Im}\,\tilde{\Omega}_1$ (dotted), $\mathrm{Im}(\tilde{\Omega}_1+\tilde{\Omega}_2)$ (dashed), and $\mathrm{Im}(\tilde{\Omega}_1+\tilde{\Omega}_2+\tilde{\Omega}_3)$ (long dashes). Here, the horizontal axis is the normalized position x_S/L of the midpoint of the stack. The numbered points in this figure will be explained later. As mentioned before and in Eq. (B21) of Appendix B, here we evaluate $f_{V,K}$ at the value of ω given by

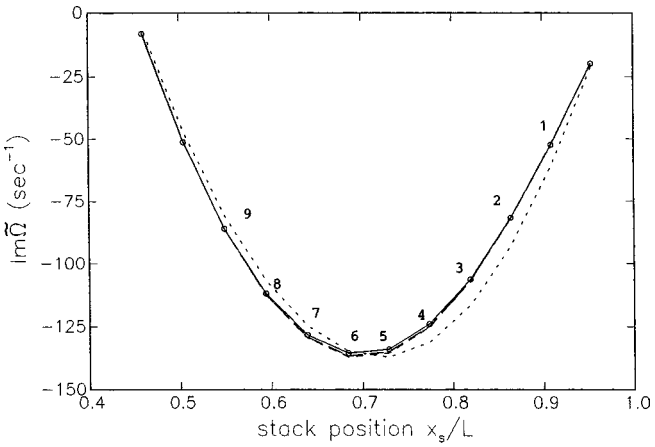

FIG. 1. Negative of the instability growth rate, i.e., imaginary part of the exact linear eigenfrequency (solid line), compared with the successive approximations Im $\tilde{\Omega}_1$ (dotted line), Im $\tilde{\Omega}_1+\tilde{\Omega}_2$ (short dashes), and Im $\tilde{\Omega}_1+\tilde{\Omega}_2+\tilde{\Omega}_3$ (long dashes) as functions of the normalized position x_S/L of the midpoint of the stack for the geometry described in the text. The temperature difference along the stack is 368 K. The numbered points are keyed to the lines in Fig. 6.

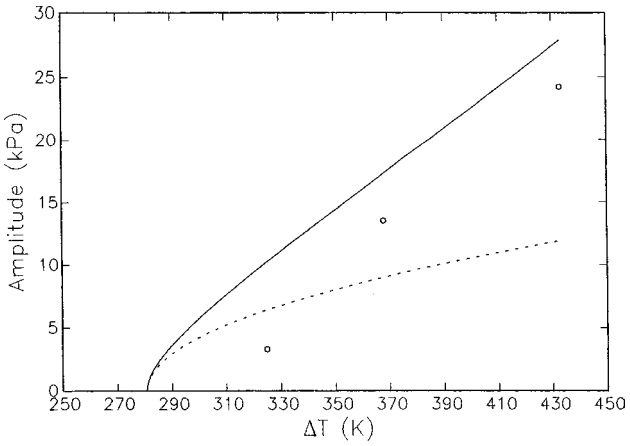

FIG. 2. Saturation amplitude of the fundamental mode (dotted line) and peak amplitude of the pressure perturbation at the cold end of the resonant tube (solid line) as a function of the temperature difference ΔT along the stack. The symbols are the data points reported by Atchley *et al.* (1990).

the first-order approximation (2.18) instead of updating it at each step of the perturbation procedure. We have verified that this simplification deteriorates the results only slightly.

We do not show any further results of this type as the earlier first-order approximation is already adequate for practical purposes and the added computational effort to go beyond it significant. Nevertheless, the fact bears mentioning as it confirms the correctness of the perturbation technique and the accuracy of the analysis. It is more interesting to focus on the chief novelty of this work, namely its nonlinear aspects.

B. Nonlinear regime

Equation (3.1), and its complex conjugate, predict the evolution of the oscillation amplitude in time. These equations can be combined to find

$$\frac{d|\tilde{A}|^2}{d\hat{t}} = -2[\mathrm{Im}\,\tilde{\Omega}_3 + \mathrm{Im}\,\tilde{\Lambda}_3|\tilde{A}|^2]|\tilde{A}|^2, \tag{3.4}$$

which is readily solved with the result

$$|\tilde{A}|^2 = \frac{|\tilde{A}|^2_{\mathrm{sat}}}{1+\exp(2\tilde{\Omega}_{3i}\hat{t})(|\tilde{A}|^2_{\mathrm{sat}}/|\tilde{A}|^2_0 - 1)}, \tag{3.5}$$

where $\tilde{A}_0$ denotes the initial value of the amplitude and

$$|\tilde{A}|^2_{\mathrm{sat}} = -\frac{\mathrm{Im}\,\tilde{\Omega}_3}{\mathrm{Im}\,\tilde{\Lambda}_3} = -\frac{\tilde{\Omega}_{3i}}{\tilde{\Lambda}_{3i}}. \tag{3.6}$$

Since $\tilde{\Omega}_{3i}<0$ for an unstable system, this equation shows that, for $\hat{t}\to\infty$, $|\tilde{A}|^2$ is asymptotic to the saturation value $|\tilde{A}|^2_{\mathrm{sat}}$ as also follows directly from the right-hand side of (3.1) since only Ω_3 and Λ_3 have nonzero imaginary parts. In the stable case, $\tilde{\Omega}_{3i}$ is positive and the amplitude decays to zero.

We begin our discussion from the asymptotic saturation amplitude $\tilde{A}_{\mathrm{sat}}$. This result is of particular interest as it contains the effect of a large number of variables such as the deviation of the temperature distribution from onset conditions, the shape of the resonator, the effect of stack geometry (through the values of the exchange parameters $f_{V,K}$) and stack length, Prandtl number, and others.

We assume a linear temperature variation between a cold temperature T_C and a hot temperature T_H in the stack, and constant temperatures equal to T_C and T_H at the left and right of the stack, respectively. We have tested two different definitions of the terms in the perturbation expansion (2.6) of T_w. In the first one we kept T_C fixed and gradually raised T_H. In the second one, we kept the average temperature along the tube constant, adjusting the temperature difference $T_H - T_C$. For the same final T_H and T_C, the two procedures gave nearly identical results as expected on the basis of the considerations of Sec. II.

We consider first the experimental situation of Atchley *et al.* (1990). The solid line in Fig. 2 is the (positive) peak amplitude as a function of the temperature difference along the stack. The dotted line shows $|\tilde{A}_{\mathrm{sat}}|$.[2] For this case our calculations indicate an onset temperature of 573.5 K which, with $T_C = 293$ K, corresponds to an onset temperature gradient of 8.01 K/mm. One recognizes here the typical structure of a supercritical bifurcation. In this figure the symbols represent the three data points reported by Atchley *et al.* (1990). In order to reconcile these data with our theoretical prediction, one would have to assume hot-end temperatures 36, 22, and 20 K lower than the reported values. We found a similar effect in our earlier numerical study (Yuan *et al.*, 1997). Two possible concurrent explanations come to mind. The first one is the temperature jump that is established between the ends of the stack and the heat exchangers, which has the effect of reducing the temperature gradient in the stack (Brewster *et al.*, 1997). Second, the temperature values reported in Atchley *et al.* were measured at the surface of the tube, rather than in the stack. As mentioned in Yuan *et al.* (1997), for the conditions of the experiment one may reasonably expect a temperature difference of this order between these

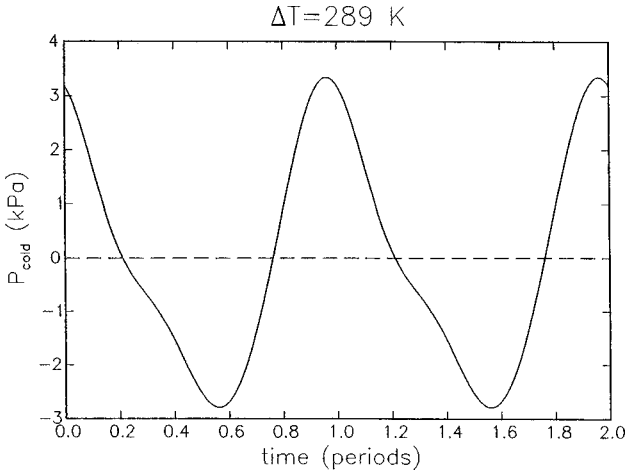

FIG. 3. Temporal waveform at the cold end of the tube for the lowest temperature case of Atchley *et al.* (1990). The temperature difference along the stack has been adjusted to 289 K so as to match the amplitude reported by Atchley *et al.* The measured period was 2.1 ms, to be compared with the present result of 1.96 ms.

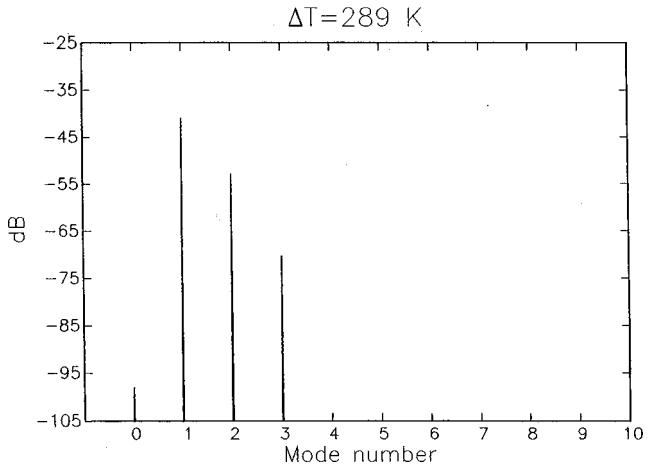

FIG. 4. Frequency spectrum for the waveform of the previous figure.

two positions. In addition, the experimental setup will most likely include several losses (e.g., due to the lack of alignment between the heat exchanger and stack plates, which causes an increase of the effective blockage of the tube, heat conduction in the gas, and others) that are not included in our model. Hence, the difference with the data is in the expected direction and of a reasonable magnitude. The discrepancy at the lowest temperature difference is somewhat larger but, on the other hand, it is here that the effect of losses would be greatest. In our earlier numerical study, where we tried to accommodate additional loss mechanisms by smoothing the cross-sectional area and wall temperature distributions, we actually found that this low-temperature case was predicted to be stable.

The temporal waveform at the cold end of the tube corresponding to the case with the lowest temperature difference along the stack is shown in Fig. 3. Here, the temperature difference has been adjusted so as to match the amplitude reported by Atchley *et al.* Upon comparing with Fig. 2 of that reference, one sees the same steepening of the wave profile and an asymmetry in the curvatures of the peaks and valleys similar to the measured one. The second harmonic is, however, slightly more prominent in our result. Figure 4 shows the calculated spectrum. The ratio of the second and third harmonics to the first one is -12 and -29 dB, respectively, to be compared with the experimental values of -16 and -32 dB. The oscillation period measured in the experiment was 2.1 ms, which is in good agreement with our result of 1.96 ms.

The saturation amplitude for the case at the next higher temperature is much larger and the data show a substantial harmonic content extending to at least the sixth harmonic. Since our method only gives results up to the third harmonic, the comparison with the measured waveform is not as satisfactory (Fig. 5). In this case the second and third harmonics are 3 and 11 dB below the fundamental, to be compared with reported values of 7.6 and 14.5. Thus, in this case as in the previous one, the second harmonic is found to be larger than the measured one. In our experience, the amplitude of this harmonic is strongly dependent on the details of the resonator geometry and it is therefore also possible that this difference is due to a mismatch between the experimental arrangement and the way it is modeled here rather than to inaccuracies of the perturbation method. The measured period was 2.1 ms, to be compared with our result of 1.96 ms.

The expressions derived before contain a dependence on many variables, the effect of which can also be studied. To produce the results that follow, the stack length was taken as 30 mm while the geometry and other parameter values were the same as before, unless otherwise noted. To reduce the number of parameters, however, we removed the heat exchangers and took the stack plates to have zero thickness so that there is no blockage of the tube's cross section. Furthermore, momentum and energy transfer with the solid structure away from the stack region were neglected.

Figure 6 shows the dependence of the (negative) peak amplitude at the cold end of the tube upon the position of the stack as a function of the temperature difference along the stack. The positions are keyed to those marked by numbers

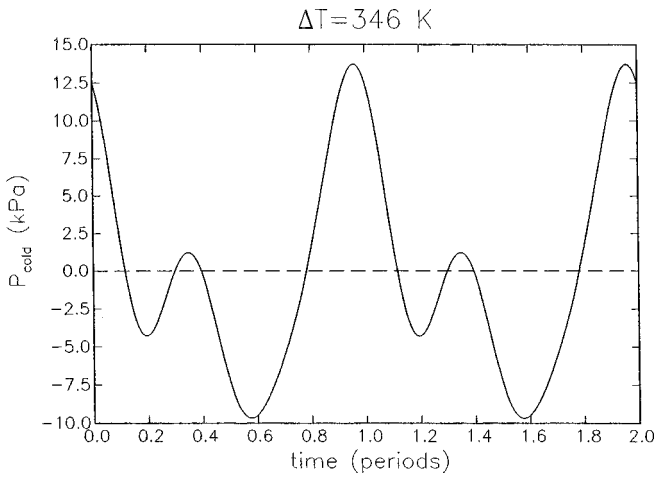

FIG. 5. Temporal waveform at the cold end of the tube for the intermediate temperature case of Atchley *et al.* (1990). The temperature difference along the stack has been adjusted to 346 K to match the amplitude reported by Atchley *et al.* The measured period was 2.1 ms, to be compared with the present result of 1.95 ms.

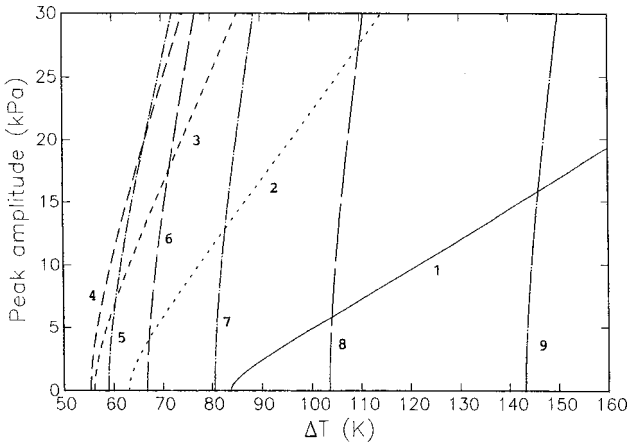

FIG. 6. Dependence of the peak amplitude at the cold end of the tube upon the position of the stack as a function of the temperature difference along the stack. The stack positions are keyed to the numbers marked in Fig. 1.

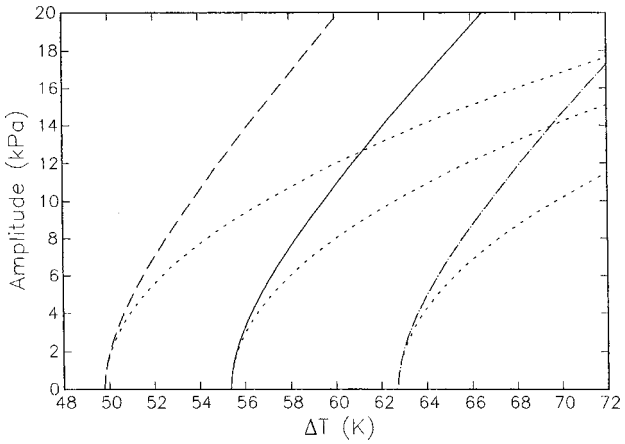

FIG. 8. Dependence of the peak amplitude at the cold end of the tube upon the gas Prandtl number σ for a stack position of $x_S/L=0.774$. From the left, the lines are for $\sigma=0.5$, 0.72, and 1.0. The dotted lines are the first-harmonic amplitude.

in Fig. 1. The strongest dependence on the temperature difference occurs near the three-quarters position along the tube as expected.

Figure 7 shows, for a stack positioned at $x_S/L=0.729$, the dependence of the (negative) peak amplitude at the cold end of the tube upon the stack-plate spacing. This is the same case considered in the linear approximation in Fig. 4 of Karpov and Prosperetti (1998). The solid line is for $\delta_K/l=0.31$, the dashed line for $\delta_K/l=0.24$, and the dash-and-dot line for $\delta_K/l=0.40$. The dotted lines are the amplitudes of the first harmonic. It can be seen that an optimal value of $\delta_K/l\simeq 0.31$ exists in this case. The value of δ_K used here is based on the first eigenvalue of (2.18) and is 0.2 mm.

The dependence on the Prandtl number is shown in Fig. 8 for a stack placed at $x_S/L=0.774$. From the left, the results are for $\sigma=0.5$, 0.72, and 1.0. The dotted lines are the first-harmonic amplitude. As expected, the smaller the Prandtl number the lower the onset temperature difference, although the slope of the lines is not very sensitive to this quantity.

The effect of the tube length L is shown in Fig. 9. The middle curve is for $L=99.89$ cm (i.e., the length used by Atchley *et al.*, 1990). The lines on the left and the right are for tube lengths of 124.86 and 84.91 cm, respectively. For all three cases, $x_S/L=0.774$. An increase in L over the range considered decreases the onset temperature gradient and destabilizes the system. This result is mainly due to the lowering of the onset gradient as shown in Eq. (51) of our earlier paper (Karpov and Prosperetti, 1998).

The model we have used can accommodate tubes with a nonuniform cross section. To illustrate this effect, we consider a tube with cross-sectional area given by

$$\frac{S(x)}{S(0)}=\begin{cases}1 & 0\leqslant \frac{1}{4}L\\ [1+Z\cos^2\pi(2x/L-1)]^2 & \frac{1}{4}L\leqslant x\leqslant\frac{3}{4}L\\ 1 & \frac{3}{4}L\leqslant x\leqslant L.\end{cases} \tag{3.7}$$

Figure 10 shows the peak amplitudes for several values of the parameter Z and $x_S/L=0.774$. For $Z>1.5\%$ the phase of the harmonics is such that the compression phase of the

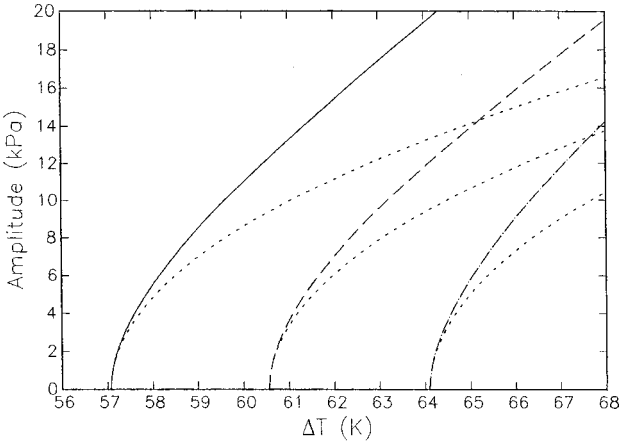

FIG. 7. Dependence of the peak amplitude at the cold end of the tube upon the dimensionless thermal penetration depth δ_K/l for a stack positioned at $x_S/L=0.729$. The solid line is for $\delta_K/l=0.31$, the dashed line for $\delta_K/l=0.24$, and the dash-and-dot line for $\delta_K/l=0.40$. The dotted lines are the amplitudes of the first harmonic.

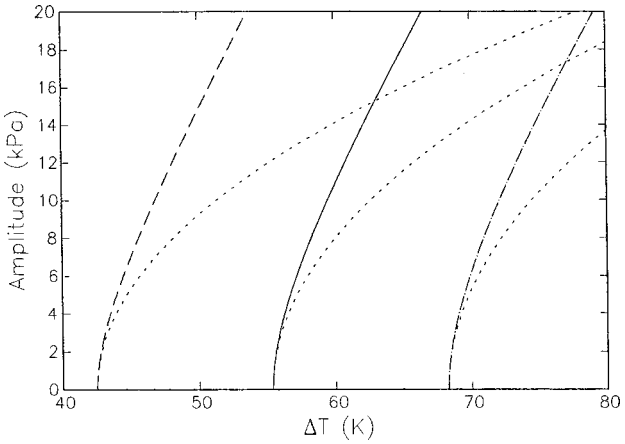

FIG. 9. Dependence of the peak amplitude at the cold end on the tube length L. The middle curve is for the length used by Atchley *et al.* (1990); the lines on the left and the right are for tube lengths 25% greater and 15% smaller. The dotted lines are the first-harmonic amplitude. In all cases, the stack is positioned at $x_S/L=0.774$.

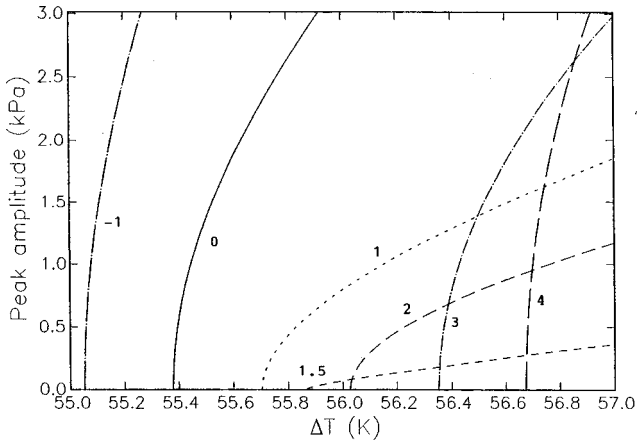

FIG. 10. Dependence of the peak amplitudes at the cold end of the tube upon the cross-sectional area variation as parametrized by the parameter Z in Eq. (3.7) expressed in percent. The stack is positioned at $x_S/L=0.774$.

wave has greater amplitude than the rarefaction phase. In this case, we show the positive peak amplitude. The reverse happens for other values of Z, for which we show the negative peak amplitude. The effect is very strong and we express Z in percent. As the cross section is widened there is a minimum occurring around $Z=1.5\%$. In these conditions the second harmonic is strongly resonant and its contribution to the spectrum is larger than that of the first harmonic. Narrowing cross sections destabilize the system, as already found earlier (Watanabe *et al.*, 1997).

The final parameter we consider is the tube diameter (Fig. 11). The middle curve is for a diameter of 38.2 mm, which is the same as used by Atchley *et al.* (1990); the lines on the left and on the right are for diameters of 45.8 and 30.6 mm, respectively. For these calculations of course we restore the exchange terms with the solid structure away from the stack region. The results show a destabilizing effect of an increasing radius. The observed effect is large because, even if the penetration depth is much less than the radius, the length of the tube is so large that the total fluid volume affected by the transfer of momentum and heat between the gas and the wall is comparable to the entire stack volume.

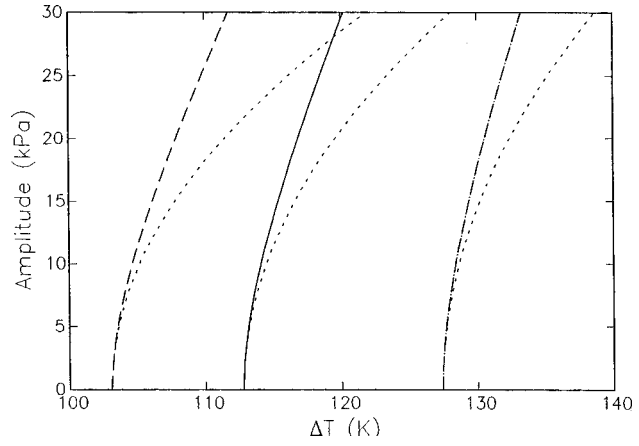

FIG. 11. Dependence of the peak amplitudes at the cold end of the tube upon the tube diameter. The middle curve is for the diameter used by Atchley *et al.* (1990); the lines on the left and the right are for diameters 20% bigger and 20% smaller. The dotted lines are the first-harmonic amplitude.

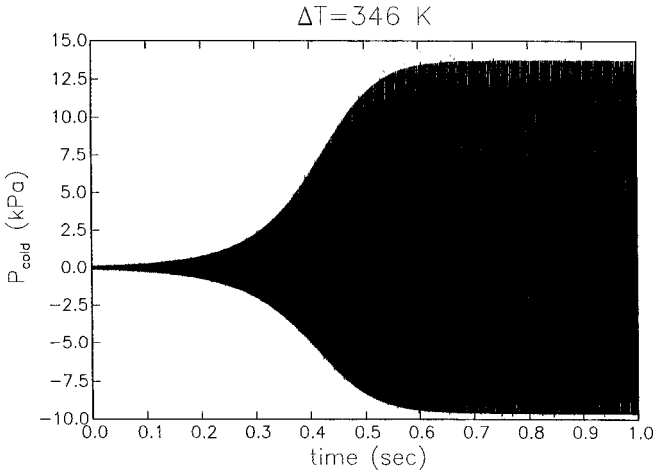

FIG. 12. Time dependence of the cold-end pressure for the middle-temperature case $\Delta T=346$ K of Atchley *et al.* (1990) considered in Fig. 5 as predicted by Eq. (3.8).

If (3.5) is substituted into (3.1), the resulting equation is readily solved and the following complete solution for $\tilde{A}(t)$ determined:

$$\frac{\tilde{A}(\hat{t})}{\tilde{A}_0}=\exp\left\{ i(\omega+\tilde{\Omega}_1+\tilde{\Omega}_2+\tilde{\Omega}_3)\hat{t}+i\frac{\tilde{\Lambda}_2+\tilde{\Lambda}_3}{2\tilde{\Lambda}_{3i}} \times\ln\left[1+\frac{|\tilde{A}|_0^2}{|\tilde{A}|_{\mathrm{sat}}^2}(\exp[-2\tilde{\Omega}_{3i}\hat{t}]-1)\right]\right\}. \tag{3.8}$$

From this expression, the time dependence of all the fields can be calculated. As an example, Fig. 12 shows the cold-end pressure versus time for the middle-temperature case of Atchley *et al.* (1990) considered in Fig. 5. The general behavior of this result is in agreement with what is observed experimentally (see, e.g., Wheatley, 1986). The early-time behavior is shown on a much magnified time scale in Fig. 13, where the dashed line shows the envelope from Eq. (3.5).

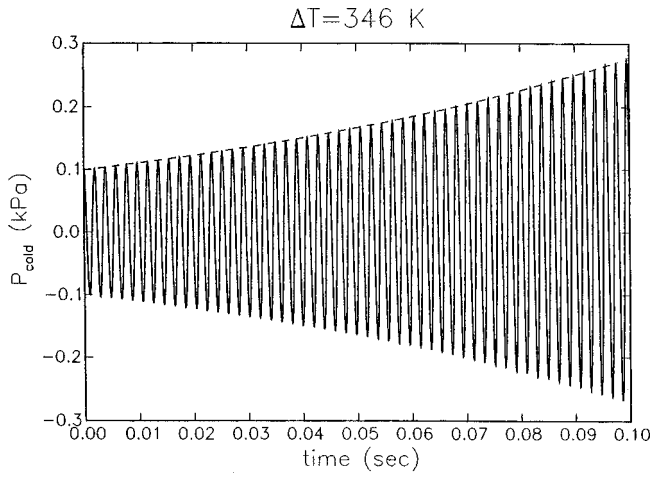

FIG. 13. Detail of the previous figure. The dashed line is the envelope from Eq. (3.5).

IV. DISCUSSION

As mentioned in Sec. I, the form of the heat and momentum transfer operators that we have used in deriving the results discussed so far is somewhat uncertain in the nonlinear domain. Furthermore, it would be of great interest to know how accurate the asymptotic results are. In this section we address—albeit partially—these important questions with the help of the somewhat different heat-transfer model used in our earlier studies and by comparing the results with the fully nonlinear calculation of Yuan *et al.* (1997).

A. Other form for the heat transfer operators

In our original model (Watanabe *et al.*, 1997), in the frequency domain the heat transfer operators $\mathcal{H}$, $\mathcal{Q}$ were given by

$$\mathcal{H}(T-T_w)=i\omega\rho_0 c_p\frac{f_K}{1-f_K}(T-T_w), \tag{4.1}$$

$$\mathcal{Q}(u)=\frac{\rho_0 c_p}{1-\sigma}\left(\frac{f_V}{1-f_V}-\frac{\sigma f_K}{1-f_K}\right)u. \tag{4.2}$$

The form (1.5) used before is found by eliminating the temperature difference $T-T_w$ using the exact linear result given in Eq. (52) of Watanabe *et al.* (1997). The two formulations are therefore precisely equivalent if the linear problem is solved exactly. However, if, as in the present method, the linear problem is not solved exactly, the results are not necessarily the same.

The method of calculation is the same as that described in the previous sections. For example, the first-order result for $\tilde{\Omega}_1$ is similar to (3.2), namely

$$\begin{aligned}\tilde{\Omega}_1=&-\frac{1}{2Vp_0^2\omega}\int_0^L dx\,S\left[c_0^2\left(\frac{f_V}{1-f_V}+\frac{\rho_{10}}{\rho_0}\right)\left(\frac{dP_1}{dx}\right)^2\right.\\&+\gamma\omega^2\frac{f_K}{1-f_K}P_1(P_1-\mathcal{R}R_1T_{w0})\\&\left.+\frac{\gamma-1}{1-\sigma}\left(\frac{f_V}{1-f_V}-\frac{\sigma f_K}{1-f_K}\right)c_pG_0P_1\frac{dP_1}{dx}\right].\end{aligned} \tag{4.3}$$

The field P_1 appearing here satisfies the same equation (2.18) found before. We omit further details, which can be found in Karpov (2000), and focus on the results.

Figure 14, where the horizontal axis is the position of the stack, compares the growth rates of the instability predicted by the model (4.1), (4.2) at different orders; the solid line is the exact linear result calculated from Rott's equation. The conditions are the same as in Fig. 1. The dotted, dashed, and long-dashed lines show the growth rate as predicted by the first-, second-, and third-order theory, respectively. Although the picture improves as the plate spacing becomes wider, a comparison with Fig. 1 shows that the model of Sec. I is superior to that of (4.1) and (4.2). The difference between the two models decreases as the plate spacing increases, but the model of Sec. I definitely appears to be more robust.

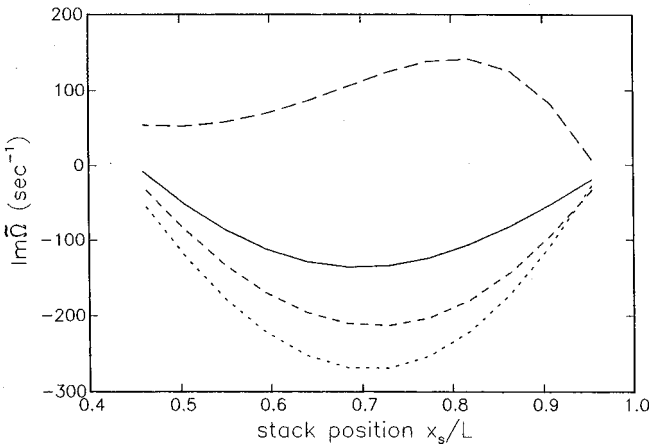

FIG. 14. Comparison of the exact linear growth rate of the instability given by Rott's model (solid line) with the first- (dotted), second- (dashed), and third-order (long dashes) results based on (4.1) and (4.2). Conditions as in Fig. 1. In this case the third-order approximation (top line) does not improve over the second-order one; it is possible that the asymptotic series does not converge. For wider gaps, however, we have found a systematic improvement as the order of the terms is increased.

B. Comparison with numerical results

In order to assess the accuracy of our perturbation method, it would be desirable to compare the results of Sec. III B with fully nonlinear numerical results based on the same model. In principle, one could think of using the approach of our earlier paper (Yuan *et al.*, 1997), in which a numerical treatment of the model of Watanabe *et al.* (1997) was given. Unfortunately, this is not possible for the reasons that we now explain.

As noted before, the model of Watanabe *et al.* (1997) differs from the one of the present paper in the use of (4.1) and (4.2) in place of (1.5). In that work, in order to convert the forms (4.1) and (4.2) to the time domain, we fixed ω to the (real) frequency of the lowest mode, and wrote the imaginary parts as time derivatives (see Yuan *et al.*, 1997 for details). If one attempts the same procedure on Eq. (1.5), the linear spectrum of the problem changes so severely that some of the higher modes become unstable. We had encountered a similar difficulty in Yuan *et al.* (1997), but there we were able to sidestep it by adding some artificial dissipation that damped this instability without much effect on the more important lower modes. We have found that it is much more difficult to reach this objective with the model of Sec. I.

For this reason, we will effect a comparison between the numerical and perturbation results based on (4.1) and (4.2). We have checked that, with a larger gap, $l/\delta_K=5.98$, the nonlinear perturbation results based on (4.1), (4.2), and (1.5) are very close. Thus, it may be expected that the error introduced by the perturbation procedure would be comparable for the two models. Again, the perturbation calculation is quite analogous to that described before and leads to an equation for the amplitude of the same form as (3.1). Explicit expressions for the quantities Ω_j, Λ_k calculated with (4.1) and (4.2) can be found in Karpov (2000).

The results of a typical comparison are shown in Fig. 15, where the line is the perturbation result and the circles the numerically calculated peak amplitudes as function of the

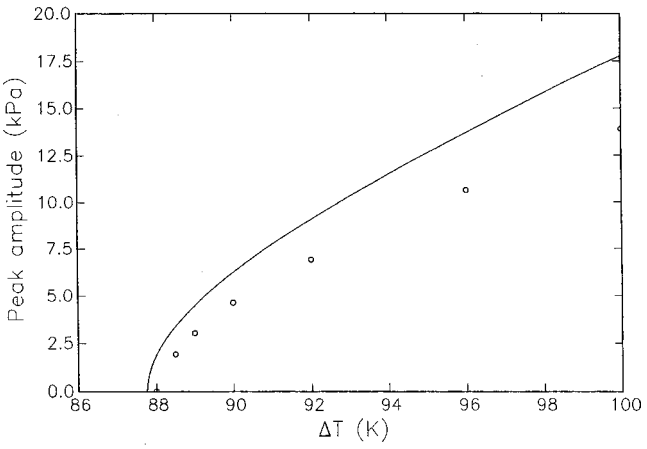

FIG. 15. Comparison between the numerically calculated peak amplitude (circles) and the perturbation results (line) as functions of the temperature difference along the stack. The dimensionless gap width is $l/\delta_K = 5.88$.

temperature difference along the stack. Here, the stack length is 30 mm and its cold end is positioned at $x_S/L = 0.774$. The gap in the stack has the value $l/\delta_K = 5.98$ and the results have been obtained by effecting the smoothing operations on $S(x)$ and $T_w(x)$ described in Yuan *et al.* (1997) 100 times. For both the analytical and the numerical results an artificial damping as described in Yuan *et al.* (1997) was used with $k_n = 0.15\,\mathrm{m}^2/\mathrm{s}$. The difference between the perturbation and numerical result increases with ΔT, as expected, but the analytical prediction is nevertheless acceptably close to the results of the numerical computations.

One last item is the following. In the model of Watanabe *et al.* (1997) the time derivatives $\partial/\partial t$ arising from the imaginary part of the heat and momentum transfer operators were transformed to a convective derivative $\partial/\partial t + u(\partial/\partial x)$ to extend the definition to the nonlinear regime. We have compared numerically the results obtained with and without the convective term $u(\partial/\partial x)$ finding very minor differences.

V. CONCLUSIONS

We have presented a time-dependent weakly nonlinear theory of the build-up of unstable oscillations in a thermoacoustic prime mover. The expressions we have derived simulate the initial growth of the instability as well as its subsequent saturation. The results are in good agreement with the limited number of experimental observations reported in the literature for the configuration that we can model.

For all the examples that we have discussed, a solution of Rott's equation shows that the imaginary part of all the modes higher than the fundamental one is positive, so that they are all stable. Therefore, the second and higher harmonic amplitudes are nonzero only due to nonlinear energy transfers from the fundamental. In the present perturbation scheme, energy transfer to the second mode starts occurring at the second order. However, the energy loss of this mode due to the coupling with the solid structure only arises at the fourth order. Since the amplitude of the fundamental saturates at a level such that the energy transferred to the second mode can be dissipated by the mechanisms affecting this mode, in order to find the saturation amplitude of the fundamental, we had to carry the expansion to this order. The fact that the perturbation method only includes a small number of modes prevents energy transfer from the fundamental to the higher modes. As a consequence, our results tend to overestimate somewhat the saturation amplitude. Nevertheless, the comparison of Sec. IV shows that there is a parameter region where the error is acceptable.

Even if our results may not be sufficiently precise in absolute terms when the temperature gradient is too far from the onset value, they are still useful for comparative purposes as they indicate trends of the system performance when design parameters or operating conditions are varied. For example, we have demonstrated the very strong effect of cross-sectional area variations. Since the expressions we have derived contain a great amount of detail on the geometry and other characteristics of the system, similar sensitivity studies with respect to other parameter variations are possible and will be pursued in the future.

In spite of the algebraic complexity of the final form of the results, the present solution is certainly much easier to evaluate than carrying out a full-fledged multidimensional *ab initio* numerical calculation. In our earlier paper (Karpov and Prosperetti, 1998) it was possible to simplify the form of the solution by using the short-stack approximation. Here, this approximation is not very useful because the result depends on auxiliary fields such as P_{21}, P_{22}, etc., the determination of which requires the solution of (B7), (B8), etc. Nevertheless, it might be possible to develop some comparable approximation, a topic that also will be pursued in future work.

ACKNOWLEDGMENT

The authors express their gratitude to the Office of Naval Research for the support of this work.

APPENDIX A: SCALING

In this Appendix we provide a justification of (2.2) and of the perturbation expansion used in the paper. For this purpose it is sufficient to consider the result (3.2) for $\tilde{\Omega}_1$; since it will be sufficient to stop at this order in ϵ, we omit the term ρ_{10}/ρ_0 thus dealing, in effect, with the linear case already studied in our earlier paper [Karpov and Prosperetti, 1998, Eq. (32)]

$$\tilde{\Omega}_1 = -\frac{1}{2Vp_0^2\omega}\int_0^L dx\, S\left[c_0^2\frac{f_V}{1-f_V}\left(\frac{dP_1}{dx}\right)^2 + (\gamma-1)\right.$$
$$\left.\times\omega^2 f_K P_1^2 + \frac{(\gamma-1)(f_V-f_K)}{(1-\sigma)(1-f_V)}c_p G_0 P_1\frac{dP_1}{dx}\right]. \quad \text{(A1)}$$

If we multiply Eq. (2.18) by SP_1 and integrate over the tube length, by using the normalization (2.21) we find

$$\omega = \frac{1}{Vp_0^2\omega}\int_0^L dx\, Sc_0^2\left(\frac{dP_1}{dx}\right)^2. \quad \text{(A2)}$$

The perturbation procedure that we have used is based on the assumption that $\tilde{\Omega}_1/\omega$ is small. This ratio consists of the sum of three terms that we examine in turn. The first one is

$$N_1 = -\frac{1}{2}\frac{\int_0^L dx\, Sc_0^2[f_V/(1-f_V)](dP_1/dx)^2}{\int_0^L dx\, Sc_0^2(dP_1/dx)^2}. \tag{A3}$$

In typical thermoacoustic engines, f_V is very small away from the stack, while it is of order 1 in the stack region of length L_S. If $\overline{f_V}$ is the typical magnitude of f_V in this region, we thus have

$$N_1 \simeq \frac{\overline{f_V}}{1-\overline{f_V}}\frac{L_S}{L}. \tag{A4}$$

Thus, N_1 will be small when the relation (2.2) is verified.

For the second term,

$$N_2 = -\frac{1}{2}\frac{\int_0^L dx\, S(\gamma-1)\omega^2 f_K P_1^2}{\int_0^L dx\, Sc_0^2(dP_1/dx)^2}, \tag{A5}$$

we use the estimate

$$P_1 \sim L\frac{dP_1}{dx} \sim \frac{c_0}{\omega}\frac{dP_1}{dx}, \tag{A6}$$

to conclude in a similar way that

$$N_2 \sim (\gamma-1)\overline{f_K}\frac{L_S}{L}, \tag{A7}$$

which, again, proves the smallness of N_2 when (2.2) is verified.

Proceeding similarly in the case of the third term we note that, since $(\gamma-1)c_p = c_0^2/T_w$, the estimate (A6) leads to

$$N_3 \sim \frac{(\overline{f_V}-\overline{f_K})}{(1-\sigma)(1-\overline{f_V})}\frac{G_0}{\overline{T_w}}L_S \sim \frac{\Delta T}{\overline{T_w}}. \tag{A8}$$

Formally, this quantity is small when $\Delta T \ll \overline{T_w}$, which is seldom the case in real thermoacoustic engines. However, this is the only potentially destabilizing term and its imaginary part is therefore of the opposite sign of the contribution of the other two terms. The ΔT in this result should therefore more properly be interpreted as the amount by which the temperature difference along the stack differs from its threshold value. This estimate confirms the previous statement that the present theory is applicable near onset conditions.

APPENDIX B: DETAILS OF THE CALCULATION

Here, we supply some details on the calculation with intermediate expressions that can be useful to better understand the method and check the results. For clarity, it is useful to rewrite the equations of the model casting all the nonlinear terms into the right-hand sides. The result is

$$\frac{\partial \rho'}{\partial \hat{t}} + \frac{1}{S}\frac{\partial}{\partial x}(S\rho_0 u') = -\frac{1}{S}\frac{\partial}{\partial x}(S\rho' u'), \tag{B1}$$

$$\rho_0\frac{\partial u'}{\partial \hat{t}} + \frac{\partial p'}{\partial x} = -\rho'\frac{\partial u'}{\partial t} - (\rho_0+\rho')u'\frac{\partial u'}{\partial x} - \mathcal{D}(u'), \tag{B2}$$

$$\frac{\partial p'}{\partial \hat{t}} + \frac{\gamma p_0}{S}\frac{\partial (Su')}{\partial x} = -u'\frac{\partial p'}{\partial x} - \frac{\gamma p'}{S}\frac{\partial (Su')}{\partial x} + (\gamma-1) \times [\mathcal{T}(p',u') + u'\mathcal{D}(u')]. \tag{B3}$$

Note that the gas temperature is not involved in these equations. At each step of the perturbation procedure this quantity can be determined from the equation of state (1.4).

As in Sec. II, we separate the different steps in the perturbation method.

A. Second order

At second order, Eqs. (B1)–(B3) give

$$\frac{\partial \rho_2}{\partial t} + \frac{1}{S}\frac{\partial}{\partial x}(S\rho_0 u_2) = -\frac{\partial \rho_1}{\partial \tau} - \frac{1}{S}\frac{\partial (S\rho_1 u_1)}{\partial x}, \tag{B4}$$

$$\rho_0\frac{\partial u_2}{\partial t} + \frac{\partial p_2}{\partial x} = -\mathcal{D}_1 - \rho_0\left(\frac{\partial u_1}{\partial \tau} + u_1\frac{\partial u_1}{\partial x}\right) - \rho_1\frac{\partial u_1}{\partial t}, \tag{B5}$$

$$\frac{\partial p_2}{\partial t} + \frac{\gamma p_0}{S}\frac{\partial (Su_2)}{\partial x} = (\gamma-1)\mathcal{T}_1 - \frac{\partial p_1}{\partial \tau} - u_1\frac{\partial p_1}{\partial x} - \frac{\gamma p_1}{S}\frac{\partial}{\partial x}(Su_1). \tag{B6}$$

The second and third equations can be combined to give the single equation (2.26) for p_2 by taking the derivative with respect to time of (B6) and using (B5) to eliminate $\partial u_2/\partial t$.

The functions P_{21}, P_{22}, and P_{20} appearing in the expansion (2.32) of p_2 satisfy the equations

$$\frac{1}{S}\frac{d}{dx}\left(c_0^2 S\frac{dP_{21}}{dx}\right) + \omega^2 P_{21} = -2\omega\Omega_1 P_1 - (\gamma-1)\omega^2 F_K P_1 - (\gamma-1)c_p F_Q G_0\frac{dP_1}{dx} + \frac{1}{S}\frac{d}{dx}\left[Sc_0^2\left(F_D + \frac{\rho_{10}}{\rho_0}\right)\frac{dP_1}{dx}\right], \tag{B7}$$

$$\frac{1}{S}\frac{d}{dx}\left(c_0^2 S\frac{dP_{22}}{dx}\right) + 4\omega^2 P_{22} = -\frac{\gamma p_0}{S\omega^2}\frac{d}{dx}\left[\frac{1}{\rho_0^3}\frac{d(S\rho_0)}{dx}\left(\frac{dP_1}{dx}\right)^2\right] - 2\left[\frac{1}{\rho_0}\left(\frac{dP_1}{dx}\right)^2 - \omega^2\frac{P_1^2}{p_0}\right], \tag{B8}$$

$$\frac{dP_{20}}{dx} = -\frac{1}{S\omega^2}\frac{d}{dx}\left[\frac{S}{\rho_0}\left(\frac{dP_1}{dx}\right)^2\right]. \tag{B9}$$

The first two equations are found by substituting (2.32) into (2.26) and separating the frequency components. The last equation could also be found in the same way, but it is more convenient to obtain it from the momentum equation. The boundary conditions for all these equations are the same [(2.20)] as for P_1. Note that these conditions are automatically satisfied by P_{20}, which is then determined only up to a

constant. To make the solution unique, we impose the additional condition

$$\int_0^L S\frac{P_{20}}{T_{w0}}dx=0, \tag{B10}$$

which follows from the conservation of the total gas mass in the tube.

We write the $O(\epsilon^2)$ contribution to the gas density as

$$\rho_2=\rho_{20}+\rho_{21}+\rho_{22}, \tag{B11}$$

where the first index denotes the order in ϵ and the second one the frequency. The time-independent term ρ_{20}, however, consists of two contributions, one, ρ_{200}, due to the corrections T_{w1} and T_{w2} of the wall temperature, to be determined later, and the other, ρ_{202}, analogous to P_{20} in (2.32), that exists due to nonlinear effects.

$$\rho_{20}=\rho_{200}+A^*A\rho_{202}. \tag{B12}$$

Both quantities follow from the equation of state in the form

$$\rho_{200}=-\rho_{10}\frac{T_{w1}}{T_{w0}}-\rho_0\frac{T_{w2}}{T_{w0}},\quad \rho_{202}=2\rho_0\frac{P_{20}}{p_0}. \tag{B13}$$

The time-dependent parts of ρ_2 and u_2 have the same structure as (2.32), except that $U_{20}=0$. The spatial parts are

$$R_{21}=-\frac{\Omega_1}{\omega}R_1-\frac{1}{\omega^2 S}\frac{d}{dx}\left[S\left(\frac{dP_{21}}{dx}-\left(\frac{\Omega_1}{\omega}+F_D\right)\frac{dP_1}{dx}\right)\right], \tag{B14}$$

$$R_{22}=\frac{i}{2\omega S}\frac{d}{dx}S(\rho_0U_{22}+R_1U_1), \tag{B15}$$

$$U_{21}=\frac{i}{\omega\rho_0}\left[\frac{d\rho_{21}}{dx}-\left(F_D+\frac{\Omega_1}{\omega}+\frac{\rho_{10}}{\rho_0}\right)\frac{dP_1}{dx}\right], \tag{B16}$$

$$U_{22}=\frac{i}{2\omega\rho_0}\left[\frac{dP_{22}}{dx}+\frac{1}{\rho_0\omega^2}\left(\frac{dP_1}{dx}\right)^2\left(\frac{1}{S}\frac{dS}{dx}+\frac{1}{\rho_0}\frac{d\rho_0}{dx}\right)\right]. \tag{B17}$$

The contributions of the drag and heat transfer operators necessary for the next order split into parts at frequency ω and 2ω as

$$\mathcal{D}_2=\mathcal{D}_{21}+\mathcal{D}_{22},\quad \mathcal{T}_2=\mathcal{T}_{21}+\mathcal{T}_{22}. \tag{B18}$$

In writing $\mathcal{D}_{21}$, care must be exerted because $\mathcal{D}$ acting on

$$\begin{aligned}u_1&=B(\theta,\eta)\exp(i\omega t+i\Omega_1\tau)U_1(x)+\text{c.c.}\\&=B(\theta,\eta)\exp[i(\omega+\epsilon\Omega_1)t]U_1(x)+\text{c.c.}\end{aligned} \tag{B19}$$

gives

$$\begin{aligned}\mathcal{D}_1&=i(\omega+\epsilon\Omega_1)(\rho_0+\epsilon\rho_{10})F_DU_1B(\theta,\eta)\\&\quad\times\exp[i(\omega+\epsilon\Omega_1)t]+\text{c.c.}\end{aligned} \tag{B20}$$

The terms containing ϵ have properly been disregarded in writing the form (2.12) of $\mathcal{D}_1$ for use with the second-order problem. However, this term contributes to the next order and therefore it must be restored. We include it in the definition of $\mathcal{D}_{21}$ and $\mathcal{T}_{21}$, and we thus find

$$\begin{aligned}\mathcal{D}_{21}&=iF_D[\rho_0\omega U_{21}+(\rho_0\Omega_1+\rho_{10}\omega)U_1]B(\theta,\eta)\\&\quad\times\exp[i(\omega+\epsilon\Omega_1)t]+\text{c.c.}\\&=-iF_D\left[\frac{dP_{21}}{dx}-F_D\frac{dP_1}{dx}\right]B(\theta,\eta)\\&\quad\times\exp[i(\omega+\epsilon\Omega_1)t]+\text{c.c.}\end{aligned} \tag{B21}$$

Strictly speaking, the definition of f_V should also be modified to contain $\omega+\epsilon\Omega_1$, rather than ω. However, in the range of practical interest, the derivative of f_V with respect to ω is small and the correction numerically not very important. We therefore disregard it for simplicity. The component at frequency 2ω is

$$\mathcal{D}_{22}=2i\omega\rho_0F_{2D}U_{22}A^2(\tau,\theta,\eta)\exp(2i\omega t)+\text{c.c.}, \tag{B22}$$

where we write F_{2D} as a reminder that ω should be replaced by 2ω in the definition (1.5). Similarly, we have

$$\begin{aligned}\mathcal{T}_{21}&=[-i\omega F_KP_{21}-i\Omega_1F_KP_1-c_pF_Q(\rho_0G_0U_{21}\\&\quad+\rho_{10}G_0U_1+\rho_0G_1U_1)]B(\theta,\eta)\exp[i(\omega+\epsilon\Omega_1)t]\\&\quad+\text{c.c.},\end{aligned} \tag{B23}$$

$$\begin{aligned}\mathcal{T}_{22}&=[-i2\omega F_{2K}P_{22}-\rho_0c_pF_{2Q}G_0U_{22}]A^2(\tau,\theta,\eta)\\&\quad\times\exp(2i\omega t)+\text{c.c.}\end{aligned} \tag{B24}$$

B. Third order

At the third order Eqs. (1.1)–(1.3) give

$$\begin{aligned}\frac{\partial\rho_3}{\partial t}+\frac{1}{S}\frac{\partial}{\partial x}(S\rho_0u_3)&=-\frac{\partial\rho_1}{\partial\theta}-\frac{\partial\rho_2}{\partial\tau}\\&\quad-\frac{1}{S}\frac{\partial}{\partial x}(S\rho_1u_2+S\rho_2u_1),\end{aligned} \tag{B25}$$

$$\begin{aligned}\rho_0\frac{\partial u_3}{\partial t}+\frac{\partial p_3}{\partial x}&=-\mathcal{D}_2-\rho_0\left(\frac{\partial u_1}{\partial\theta}+\frac{\partial u_2}{\partial\tau}+u_1\frac{\partial u_2}{\partial x}+u_2\frac{\partial u_1}{\partial x}\right)\\&\quad-\rho_1\left(\frac{\partial u_1}{\partial\tau}+\frac{\partial u_2}{\partial t}+u_1\frac{\partial u_1}{\partial x}\right)-\rho_2\frac{\partial u_1}{\partial t},\end{aligned} \tag{B26}$$

$$\begin{aligned}\frac{\partial p_3}{\partial t}+\frac{\gamma p_0}{S}\frac{\partial(Su_3)}{\partial x}&=(\gamma-1)(\mathcal{T}_2+u_1\mathcal{D}_1)-\frac{\partial p_1}{\partial\theta}-\frac{\partial p_2}{\partial\tau}\\&\quad-u_1\frac{\partial p_2}{\partial x}-u_2\frac{\partial p_1}{\partial x}-\frac{\gamma p_1}{S}\frac{\partial(Su_2)}{\partial x}\\&\quad-\frac{\gamma p_2}{S}\frac{\partial(Su_1)}{\partial x},\end{aligned} \tag{B27}$$

from which (2.33) is obtained by eliminating $\partial u_3/\partial t$

between the second and third equations.

The equations for $P_{311}(x)$, $P_{313}(x)$, $P_{32}(x)$, and $P_{30}(x)$ are obtained from Eq. (2.33) upon separating the different frequency and amplitude components in the right-hand side; P_{20} is more easily determined from the momentum equation (B26). The results are

$$\frac{1}{S}\frac{d}{dx}\left(c_0^2 S\frac{dP_{311}}{dx}\right)+\omega^2 P_{311}=-2\omega\Omega_2 P_1-2\omega\Omega_1 P_{21}-\Omega_1^2 P_1-(\gamma-1)\left[\omega F_K(2\Omega_1 P_1+\omega P_{21})\right.$$
$$\left.+c_p F_Q G_0\left(\frac{dP_{21}}{dx}-F_D\frac{dP_1}{dx}\right)+c_p F_Q G_1\frac{dP_1}{dx}\right]$$
$$+\frac{1}{S}\frac{d}{dx}\left(Sc_0^2\left[\left(F_D+\frac{\rho_{10}}{\rho_0}\right)\frac{dP_{21}}{dx}-\left(F_D^2+F_D\frac{\rho_{10}}{\rho_0}+\frac{T_{w2}}{T_{w0}}\right)\frac{dP_1}{dx}\right]\right), \tag{B28}$$

$$\frac{1}{S}\frac{d}{dx}\left(c_0^2 S\frac{dP_{313}}{dx}\right)+\omega^2 P_{313}=-2\omega\Lambda_2 P_1+i\omega\left[U_1\left(2\frac{dP_{20}}{dx}-\frac{dP_{22}}{dx}\right)+U_{22}\frac{dP_1}{dx}+\frac{\gamma P_1}{S}\frac{d(SU_{22})}{dx}\right.$$
$$\left.+\frac{\gamma}{S}(2P_{20}-P_{22})\frac{d(SU_1)}{dx}\right]+\frac{\gamma p_0}{S}\frac{d}{dx}\left[S\left(\frac{d(U_1U_{22})}{dx}+\frac{R_1}{\rho_0}\left(U_1\frac{dU_1}{dx}-2i\omega U_{22}\right)\right.\right.$$
$$\left.\left.-\left(\frac{R_{22}}{\rho_0}+2\frac{P_{20}}{p_0}\right)i\omega U_1\right)\right], \tag{B29}$$

$$\frac{1}{S}\frac{d}{dx}\left(c_0^2 S\frac{dP_{32}}{dx}\right)+4\omega^2 P_{32}=-4\omega\Omega_1 P_{22}-(\gamma-1)\left[4\omega^2 F_{2K}P_{22}-2i\omega c_p\rho_0 F_{2Q}G_0U_{22}+\frac{2}{\rho_0}F_D\left(\frac{dP_1}{dx}\right)^2\right]$$
$$-2i\omega\frac{\gamma p_0}{S}\frac{d}{dx}(SF_{2D}U_{22})+2i\omega\left[U_1\frac{dP_{21}}{dx}+U_{21}\frac{dP_1}{dx}+\frac{\gamma P_1}{S}\frac{d(SU_{21})}{dx}+\frac{\gamma P_{21}}{S}\frac{d(SU_1)}{dx}\right]$$
$$-\frac{1}{S}\frac{d}{dx}\left[Sc_0^2\left(2i\Omega_1\rho_0U_{22}+\rho_0\frac{d(U_1U_{21})}{dx}+i\omega R_1U_{21}+2i\omega\rho_{10}U_{22}+i\Omega_1R_1U_1\right.\right.$$
$$\left.\left.+\rho_{10}U_1\frac{dU_1}{dx}+i\omega R_{21}U_1\right)\right], \tag{B30}$$

$$\frac{1}{S}\frac{d}{dx}\left(c_0^2 S\frac{dP_{33}}{dx}\right)+9\omega^2 P_{33}=3i\omega\left[U_1\frac{dP_{22}}{dx}+U_{22}\frac{dP_1}{dx}+\frac{\gamma P_1}{S}\frac{d(SU_{22})}{dx}+\frac{\gamma P_{22}}{S}\frac{d(SU_1)}{dx}\right]$$
$$-\frac{1}{S}\frac{d}{dx}\left[Sc_0^2\left(\rho_0\frac{d(U_1U_{22})}{dx}+2i\omega R_1U_{22}+R_1U_1\frac{dU_1}{dx}+i\omega R_{22}U_1\right)\right], \tag{B31}$$

$$\frac{dP_{30}}{dx}=\rho_0\frac{d(U_1U_{21})}{dx}-i\omega R_1U_{21}-i\Omega_1R_1U_1+\rho_{10}U_1\frac{dU_1}{dx}-i\omega R_{21}U_1. \tag{B32}$$

$P_{30}(x)$ is complex in general, but we only need its real part $\mathrm{Re}\,P_{30}(x)$ as will be seen later. The solution for $\mathrm{Re}\,P_{30}(x)$ is made unique by means of the additional condition

$$\int_0^L\frac{S}{T_{w0}}\left(\mathrm{Re}\,P_{30}+P_{20}\frac{\rho_{10}}{\rho_0}\right)dx=0, \tag{B33}$$

that follows from the conservation of mass in the tube as in (B10).

The velocity and density fields have expressions similar to (2.40) with the spatial parts given by

$$U_{311}=\frac{i}{\rho_0\omega}\frac{dP_{311}}{dx}-\left(\frac{\Omega_2}{\omega}+\frac{\Omega_1}{\omega}\frac{\rho_{10}}{\rho_0}+\frac{\rho_{200}}{\rho_0}\right)U_1$$
$$-\left(\frac{\Omega_1}{\omega}+\frac{\rho_{10}}{\rho_0}\right)U_{21}-\frac{iF_D}{\rho_0\omega}\left(\frac{dP_{21}}{dx}-F_D\frac{dP_1}{dx}\right), \tag{B34}$$

$$U_{313}=\frac{i}{\rho_0\omega}\frac{dP_{313}}{dx}-\left(\frac{\Lambda_2}{\omega}+2\frac{P_{20}}{p_0}+\frac{R_{22}}{\rho_0}\right)U_1$$
$$-\frac{i}{\omega}\frac{d(U_1U_{22})}{dx}-2\frac{R_1}{\rho_0}U_{22}-\frac{i}{\omega}\frac{R_1}{\rho_0}U_1\frac{dU_1}{dx}, \tag{B35}$$

$$U_{32}=\frac{i}{2\omega\rho_0}\frac{dP_{32}}{dx}-\left(\frac{\Omega_1}{\omega}+\frac{\rho_{10}}{\rho_0}+F_D\right)U_{22}-\frac{1}{2}\frac{R_1}{\rho_0}U_{21}$$
$$-\frac{1}{2}\left(\frac{\Omega_1}{\omega}\frac{R_1}{\rho_0}+\frac{R_{21}}{\rho_0}\right)U_1+\frac{i}{2\omega}\frac{d(U_1U_{21})}{dx}$$
$$+\frac{i}{2\omega}\frac{\rho_{10}}{\rho_0}U_1\frac{dU_1}{dx}, \tag{B36}$$

$$U_{30}=-\frac{R_1}{\rho_0}\mathrm{Re}\,U_{21}+i\frac{U_1}{\rho_0}\mathrm{Im}\,R_{21}, \tag{B37}$$

This result for U_{30} follows from the condition that the time-independent part of the flow in the tube vanishes at every order. Furthermore

$$R_{311}=-\frac{\Omega_1}{\omega}R_{21}-\frac{\Omega_2}{\omega}R_1+\frac{i}{\omega S}\frac{d}{dx}$$
$$\times[S(\rho_0U_{311}+\rho_{10}U_{21}+\rho_{200}U_1)], \tag{B38}$$

$$R_{313}=-\frac{\Lambda_2}{\omega}R_1+\frac{i}{\omega S}\frac{d}{dx}[S(\rho_0U_{313}+R_1U_{22}$$
$$+(\rho_{202}-R_{22})U_1)], \tag{B39}$$

$$R_{32}=-\frac{\Omega_1}{\omega}R_{22}+\frac{i}{2\omega S}\frac{d}{dx}[S(\rho_0U_{32}+\rho_{10}U_{22}+R_1U_{21}$$
$$+R_{21}U_1)]. \tag{B40}$$

Again,

$$\rho_3=\rho_{30}+\rho_{31}+\rho_{32}+\rho_{33}, \tag{B41}$$

and

$$\rho_{30}=\rho_{300}+A^*A\rho_{302}, \tag{B42}$$

where

$$\rho_{300}=\rho_{10}\left(\frac{\rho_{200}}{\rho_0}-\frac{T_{w2}}{T_{w0}}\right),\quad \rho_{302}=\rho_0\frac{P_{30}}{p_0}+\rho_{10}\frac{P_{20}}{p_0}+\text{c.c.} \tag{B43}$$

For $\mathcal{T}_{31}$ and $\mathcal{D}_{31}$ we have, respectively,

$$\mathcal{D}_{31}=i\omega F_D\left\{\rho_0U_{311}+\left(\rho_{10}+\rho_0\frac{\Omega_1}{\omega}\right)U_{21}\right.$$
$$+\left(\rho_{200}+\rho_{10}\frac{\Omega_1}{\omega}+\rho_0\frac{\Omega_2}{\omega}\right)U_1+A^*A\left[\rho_0U_{313}\right.$$
$$\left.\left.+\left(\rho_{202}+\rho_0\frac{\Lambda_2}{\omega}\right)U_1\right]\right\}A(\tau,\theta,\eta)\exp(i\omega t)+\text{c.c.}, \tag{B44}$$

$$\mathcal{T}_{31}=-[iF_K(\omega P_{311}+\Omega_1P_{21}+\Omega_2P_1)$$
$$+c_pF_Q(G_0(\rho_0U_{311}+\rho_{10}U_{21}+\rho_{200}U_1)$$
$$+G_1(\rho_0U_{21}+\rho_{10}U_1)+\rho_0G_2U_1)$$
$$+A^*A\{iF_K(\omega P_{313}+\Lambda_2P_1)+c_pF_QG_0(\rho_0U_{313}$$
$$+\rho_{202}U_1)\}]A(\tau,\theta,\eta)\exp(i\omega t)+\text{c.c.} \tag{B45}$$

C. Fourth order

At fourth order Eqs. (1.2)–(1.3) give

$$\rho_0\frac{\partial u_4}{\partial t}+\frac{\partial p_4}{\partial x}$$
$$=-\mathcal{D}_3-\rho_0\left(\frac{\partial u_1}{\partial\eta}+\frac{\partial u_2}{\partial\theta}+\frac{\partial u_3}{\partial\tau}+u_1\frac{\partial u_3}{\partial x}+u_2\frac{\partial u_2}{\partial x}\right.$$
$$\left.+u_3\frac{\partial u_1}{\partial x}\right)-\rho_1\left(\frac{\partial u_1}{\partial\theta}+\frac{\partial u_2}{\partial\tau}+\frac{\partial u_3}{\partial t}+u_1\frac{\partial u_2}{\partial x}+u_2\frac{\partial u_1}{\partial x}\right)$$
$$-\rho_2\left(\frac{\partial u_2}{\partial t}+\frac{\partial u_1}{\partial\tau}+u_1\frac{\partial u_1}{\partial x}\right)-\rho_3\frac{\partial u_1}{\partial t}, \tag{B46}$$

$$\frac{\partial p_4}{\partial t}+\frac{\gamma p_0}{S}\frac{\partial(Su_4)}{\partial x}$$
$$=(\gamma-1)(\mathcal{T}_3+u_1\mathcal{D}_2+u_2\mathcal{D}_1)-\frac{\partial p_1}{\partial\eta}-\frac{\partial p_2}{\partial\theta}-\frac{\partial p_3}{\partial\tau}$$
$$-u_1\frac{\partial p_3}{\partial x}-u_2\frac{\partial p_2}{\partial x}-u_3\frac{\partial p_1}{\partial x}$$
$$-\frac{\gamma}{S}\left[p_1\frac{\partial(Su_3)}{\partial x}+p_2\frac{\partial(Su_2)}{\partial x}+p_3\frac{\partial(Su_1)}{\partial x}\right]. \tag{B47}$$

Upon eliminating $\partial u_4/\partial t$ between the second and the third one we find (2.41).

[1]More precisely, one could determine a value of T^*_{w2} corresponding to marginal stability, after which the difference $T_w(x)-[T_{w0}(x)+\epsilon T_{w1}(x)+\epsilon^2T^*_{w2}]$ would be the driving force for the instability.

[2]Since the pressure perturbation is the sum of two complex conjugate quantities, the dotted line actually shows $2|\mathrm{Re}\,\tilde{A}_{\mathrm{sat}}|$.

Akhavan, R., Kamm, R. D., and Shapiro, A. H. (**1991**). ''An investigation of transition to turbulence in bounded oscillatory Stokes flows. I. Experiment,'' J. Fluid Mech. **225**, 395–422.

Atchley, A. A., Bass, H. E., and Hofler, T. J. (**1990**). ''Development of nonlinear waves in a thermoacoustic prime mover,'' in *Frontiers in Nonlinear Acoustics*, edited by M. F. Hamilton and D. T. Blackstock (Elsevier, New York), pp. 603–608.

Brewster, J. R., Raspet, R., and Bass, H. E. (**1997**). ''Temperature discontinuities between elements of thermoacoustic devices,'' J. Acoust. Soc. Am. **102**, 3355–3360.

Cao, N., Olson, J. R., Swift, G. W., and Chen, S. (**1996**). ''Energy flux density in a thermoacoustic couple,'' J. Acoust. Soc. Am. **99**, 3456–3464.

Cooper, W. L., Yang, K. T., and Nee, V. W. (**1993**). ''Fluid mechanics of oscillatory modulated flows and associated applications in heat and mass transfer—A review,'' J. Energy Heat Mass Transfer **15**, 1–19.

Gopinath, A., Tait, N. L., and Garrett, S. L. (**1998**). ''Thermoacoustic streaming in a resonant channel: The time-averaged temperature distribution,'' J. Acoust. Soc. Am. **103**, 1388–1405.

Hinch, E. J. (**1991**). *Perturbation Methods* (Cambridge University Press, Cambridge).

Karpov, S. (**2000**). ''Nonlinear Phenomena in Thermoacoustics and Bubbly Liquids,'' Ph.D. thesis, Johns Hopkins University.

Karpov, S., and Prosperetti, A. (**1998**). ''Linear thermoacoustic instability in the time domain,'' J. Acoust. Soc. Am. **103**, 3309–3317.

Kevorkian, J., and Cole, J. D. (**1996**). *Perturbation Methods in Applied Mathematics*, 2nd ed. (Springer, New York).

Morse, P. M., and Feshbach, H. (**1953**). *Methods of Theoretical Physics* (McGraw-Hill, New York).

Murdock, J. A. (**1991**). *Perturbations* (Wiley, New York).

Naylor, A. W., and Sell, G. R. (**1982**). *Linear Operator Theory in Engineering and Science* (Springer, New York), p. 502.

Rott, N. (**1969**). ''Damped and thermally driven acoustic oscillations in wide and narrow tubes,'' Z. Angew. Math. Phys. **20**, 230–243.

Rott, N. (**1976**). ''Thermally driven acoustic oscillations. IV. Tubes with variable cross section,'' Z. Angew. Math. Phys. **27**, 197–224.
Rott, N. (**1980**). ''Thermoacoustics,'' Adv. Appl. Mech. **20**, 135–175.
Rott, N. (**1983**). ''Thermally driven acoustic oscillations, VI. Excitation and power,'' Z. Angew. Math. Phys. **34**, 609–626.
Swift, G. W. (**1988**). ''Thermoacoustic engines,'' J. Acoust. Soc. Am. **84**, 1145–1180.
Watanabe, M., Prosperetti, A., and Yuan, H. (**1997**). ''A simplified model for linear and nonlinear processes in thermoacoustic prime movers. I. Model and linear theory,'' J. Acoust. Soc. Am. **102**, 3484–3496.
Wheatley, J. (**1986**). ''Intrinsically irreversible or natural heat engines,'' in *Frontiers in Physical Acoustics*, edited by D. Sette (North-Holland, Amsterdam), pp. 35–475.
Worlikar, A. S., and Knio, O. M. (**1996**). ''Numerical simulation of a thermoacoustic refrigerator. I. Unsteady adiabatic flow around the stack,'' J. Comput. Phys. **127**, 424–451.
Worlikar, A. S., and Knio, O. M. (**1999**). ''Numerical study of oscillatory flow and heat transfer in a loaded thermoacoustic stack,'' Numer. Heat Transfer **A35**, 49-65.
Worlikar, A. S., Knio, O. M., and Klein, R. (**1998**). ''Numerical simulation of a thermoacoustic refrigerator. II. Stratified flow around the stack,'' J. Comput. Phys. **144**, 299–324.
Yuan, H., Karpov, S., and Prosperetti, A. (**1997**). ''A simplified model for linear and nonlinear processes in thermoacoustic prime movers. II. Nonlinear oscillations,'' J. Acoust. Soc. Am. **102**, 3497–3506.